Adaptive Q-control for Tapping-mode Nano Scanning Using a Piezo-actuated Bimorph Probe

by

İhsan Günev

A Thesis Submitted to the
Graduate School of Engineering
in Partial Fulfillment of the Requirements for
the Degree of

Master of Science
in
Mechanical Engineering

Koc University
November 2006

Koc University

Graduate School of Sciences and Engineering

This is to certify that I have examined this copy of a master's thesis by

İhsan Günev

and have found that it is complete and satisfactory in all respects,

and that any and all revisions required by the final

examining committee have been made.

Committee Members:

____

Çağatay Başdoğan, Ph. D. (Advisor)

____

Hakan Ürey, Ph. D.

____

Alper Tunga Erdoğan, Ph. D.

____

Levent Güvenç, Ph. D.

Date: ______________________

ABSTRACT

A new approach, called Adaptive Q-control, for tapping-mode Atomic Force Microscopy (AFM) is introduced and implemented on a home-made AFM set-up utilizing a Laser Doppler Vibrometer (LDV) and a piezo-actuated bimorph probe. In the standard Q-control, the effective Q-factor of the scanning probe is set prior to the scanning depending on the application. However, there is a trade-off in choosing the effective Q-factor of an AFM probe. The Q-factor is either increased to reduce the tapping forces or decreased to maximize the scan speed. Achieving these two benefits simultaneously using the standard Q-control is not possible. In adaptive Q-control, the Q-factor of the probe is set to a value initially as in standard Q-control, but then modified on the fly during scanning when necessary. In this paper, we present the basic theory behind the adaptive Q-control, the electronics enabling on-line modification of the effective Q-factor of the piezo-actuated probe, and the results of the scanning experiments comparing three different methods: a) without Q-control, b) with the standard Q-control, and c) with the adaptive Q-control. The results show that the performance of the adaptive Q-control is superior to the other two methods.

ÖZET

Piezo-elektrik tahrikli bir probun titreşimlerinin, Lazer doppler hızölçer ile ölçülmesi prensibine dayanarak çalışan bir Atomik Kuvvet Mikroskobu (AKM) düzeneği geliştirilmiş ve üzerinde yeni geliştirilen "uyarlanır (Adaptif) Q-kontrolü" adı verilen bir kontrol yöntemi uygulamalı olarak denenmiştir. Standart Q-kontrolü yönteminde, taramada kullanılan probunun etkin (efektif) Q değeri, tarama öncesinde belirlenmekte ve tarama boyunca sabitlenmektedir. Fakat, Q değerinin seçilmesinde her zaman bir ödünleşim söz konusudur. Standart Q-kontrolünde, probun etkin Q değeri, titreşen iğne ile taranan örnek arasında oluşan kuvvetlerin düşük olmasını sağlamak amacıyla yükseltilmekte ya da gerçeklenebilecek en yüksek tarama hızının artması için düşürülmektedir. Standart Q-kontrolu yöntemi kullanılarak bu iki faydanın eşanlı olarak kazanılması mümkün değildir. Önerilen uyarlanır (adaptif) Q-kontrolü yönteminde, probun etkin Q-değeri, standart Q-kontrolü yöntemindeki gibi tarama öncesinde istenen değere sabitlenmekte, fakat tarama sırasında gerekli durumlarda değiştirilmektedir. Bu çalışmada, uyarlanır (adaptif) Q-kontrolü'nün temel prensipleri ve teorisi tanıtılmış, piezo-elektrik tahrikli probun etkin Q değerinin gerçek zamanlı olarak değiştirilmesine olanak sağlayan elektronik donanım incelenmiş, ve son olarak 3 değişik tarama metoduna ait deney sonuçları (profiller) karşılaştırılmıştır; a) Q-kontrolsüz tarama b) standard Q-kontrolü ile tarama ve c) adaptiv Q-kontrolü ile tarama. Sonuçlar uyarlanır (adaptiv) Q kontrol yönteminin diğer 2 yöntemden üstün sonuçlar verdiğini göstermiştir.

ACKNOWLEDGEMENTS

I would like to express my sincere gratitude to my thesis advisor Dr. Cagatay Basdogan for giving me the opportunity to carry out this thesis within his research team. I appreciate Koc University College of Engineering for supporting me through education grants.

I would like to thank Dr. Hakan Urey and Dr. Erdem Alaca for giving me the opportunity working in their labs and using their equipment and of course to Prof. Dr. Levent Guvenc for his collaboration during the second part of the project.

In this long journey, I had the chance to meet with many people and experience a wonderful two and half year. I would like to thank to my dear friends Ozan Anac and Ibrahim Bukusoglu for being by my side at each step of this path. Thanks to, my precious friend Aydın Varol for his assistance during building up my experimental set-up and his friendship both during and after the lab hours, Caglar Ataman for his neverending support, Sertac Karaman for his great knowledge on control theory and for his research on adaptive Q control. The Cakallar Group Emrah Ahi, Ali Alagoz and Ugur Kaplan for their hospitability, friendship and dedicated motivation on research. My friends Yusuf Sahillioglu, Murat Otkur, Cenk Dinc, Erhan Yilmaz, and Emre Sargin for their friendship and entertaintment as housemates. Thanks to Google Inc. for leading me to quite most of the information I am searching for, and to all of the graduate students working in KU Labs for allowing me to dig and use their material stock. Finally, I would like to thank to my dear brother Sinan Gunev, my parents Betul Gunev and Taner Gunev for their continuous support on me.

TABLE OF CONTENTS

LIST OF TABLES

LIST OF FIGURES

Chapter 1

INTRODUCTION

Nanotechnology has been a hot topic as a promising technology for the next century. Imaging at nano-scale is the key issue that will widen up the manufacturing technologies and nano-electro-mechanical systems applications. These systems will be extremely fast and efficient and they are expected to have important applications like tera-byte capacity memories, DNA-computers, quantum computers, and nano scale robots. Atomic Force microscope (AFM), also known as Scanning Force Microscopy (SFM), is a tool that is used for imaging of nano-scale surfaces with atomic resolution [1]. In AFM, a micro-fabricated cantilever shaped probe with a sharp tip underneath is used to scan substrate surface. The combination of attractive and repulsive interaction forces between the tip and the substrate causes the free end of the probe to deflect. Through a measurement feedback and Z positioning of the substrate, 3D topographic map of the substrate surface can be obtained. Moreover, nano-indentation, scratch, and wear tests can be performed and material properties such as elasticity and hardness can be extracted from the measurements.

Control methods that speed-up the scanning process are still interest of research. However, in many commercial AFM systems, the manufacturers of the system usually do not provide access to the inside of the controller and the software. Therefore, developing and testing new control schemes on the commercial AFM setups is not always possible. In order to have an AFM setup where new control schemes can be developed and tested, we built a home-made AFM and developed a new control approach named *Adaptive Q-control*. In the standard Q-control, the effective Q-factor of the scanning probe is set prior to the scanning depending on the application. However, there is a trade-off in choosing the effective Q-factor of an AFM probe. The Q-factor is either increased to reduce the tapping forces or decreased to maximize the scan speed. Achieving these two benefits simultaneously using the standard Q-control is not possible. In adaptive Q-control, the Q-factor of the probe is set to a value initially as in standard Q-control, but then modified on the fly during scanning when necessary.

The thesis is organized as follows: Chapter 2 gives a literature survey on imaging methods at nano-scale, Atomic Force Microscopy and its operation modes, and the related control issues. In Chapter 3, mathematical modeling of a simple cantilever probe is presented. The sub-sections in the chapter are devoted to the modeling of the cantilever, to the study of the interaction forces between the probe tip and the sample in tapping mode AFM operation and modeling of the probe dynamics focusing on the theory Q-control. Next chapter (Chapter 4) summarizes our efforts in constructing a nano scanning set-up for imaging at nano scale. It describes each component used in the set-up and how they are integrated into each other. We also introduce the adaptive Q-control in this section. Chapter 5 presents the dynamical characterization of the system. The piezo actuated bimorph AFM used for scanning is characterized in order to find its spring constant, damping coefficient and mass. In addition, the operating bandwidths of each component of the AFM set-up are experimentally obtained in order to find the slowest one limiting the scan speed of the system. In Chapter 6, images taken with the developed set-up are given. The first section of this chapter presents scan images of the standard calibration grids using conventional PID control. Second section shows how the quality factor of a probe can be controlled using the set-up and the developed signal processing circuit. Third section presents the adaptive Q control and its improvement on scan performance. And in the last chapter, we compare the performance of the different control methods implemented in this study and discuss the future work.

Chapter 2

LITERATURE REVIEW

2.1 Overview

Atomic Force Microscopy (AFM) also known as Scanning Force Microscopy (SFM), introduced by Binning et al. [1], is a widely used imagining technique at both micro and nano-scale. In AFM, a micro fabricated cantilever shaped probe with a sharp tip underneath is used to scan substrate surface. The combination of attractive and repulsive interaction forces between the tip and the substrate causes the free end of the probe to deflect. Through a measurement feedback and Z positioning of the substrate, 3D topographic map of the substrate surface can be obtained. Moreover, nanoindentation, scratch, and wear tests can be performed and material properties such as elasticity and hardness can be extracted from the measurements. Using an AFM, it is also possible to manipulate nano-scale objects.

2.2 AFM Methods

Contact mode AFM (CM-AFM) introduced by Binning et al. is the very first imaging method utilized a micro cantilever probe for scanning. CM-AFM relies on pushing the cantilever against the sample surface with a piezoelectric positioning element. In this method, the deflection of the cantilever is sensed and compared to a desired value of deflection. A controller maintains desired deflection by moving the sample or the probe up and down during raster scanning of the sample surface. The main problem with the contact mode is the excessive tracking (lateral) forces applied by the probe to the sample. The effects can be reduced by minimizing tracking force of the probe on the sample, but there are practical limits to the magnitude of the force that can be controlled by the user during operation in ambient environments.

Imaging with AFM was improved using an oscillating cantilever [2, 3]. There are two different methods for the oscillating cantilever: Amplitude-Modulation Atomic Force Microscopy (AM-AFM) and Frequency-Modulation Atomic Force Microscopy (FM-AFM). In AM-AFM, the cantilever is oscillated with a frequency close to the resonant frequency and the control system driving the nano-positioning mechanism is forced to keep the amplitude of the oscillations constant whereas in the latter one the frequency of the oscillation is tracked. In FM-AFM, the change in the frequency is detected and used as a feedback signal. The AM-AFM technique can be applied in both non-contact (NC-AFM) and tapping (intermittent) modes. FM-AFM is especially suitable for non-contact mode AFM, where no physical contact with the surface occurs. The non-contact mode was first introduced by Martin et. al. [2] using the amplitude signal as feedback. A few years later the tapping-mode was introduced by Zhong et al. [4]. This mode of operation was especially applied to high-resolution imaging of biological samples, silicon surfaces, and to manipulation of nano-particles. The oscillating cantilever methods are also called Dynamic Atomic Force Microscopy (DAFM) methods. A very intensive review of this area, including the theory of DAFM and the applications, was given by Garcia and Pérez [5].

2.3 Tapping-Mode Atomic Force Microscopy

In tapping-mode AFM, a probe oscillating with constant amplitude near to its resonant frequency is scanned over the sample surface. The feedback signal is mostly the amplitude of the tip oscillations. A controller moves the sample in vertical direction such that the oscillation amplitude stays constant. The frequency or the phase of the tip oscillations can be also measured and used in the feedback loop for the analysis of the scanned surface. As the name “tapping mode” suggests, the tip of the cantilever taps for a very short time to the surface and thus it is mostly out of contact with the sample [4]. This scheme introduces very small lateral forces on the sample being imaged. The basic principle of tapping-mode AFM is shown in Figure 2.1. The cantilever is oscillated at the desired frequency and amplitude. The frequency of this driving signal is generally the resonant frequency of the cantilever. Then, the deflection of the cantilever is measured and its RMS value is fed back to a controller. The controller tries to keep the amplitude of the oscillations (thus the value of the feedback signal) constant by adjusting the sample position in vertical direction. During tapping-mode AFM, although lateral forces are reduced, tapping forces may reach to high amplitudes due to tip-sample mechanical contact and these high repulsive forces may result in extensive surface deformation especially in biological samples [6, 7].

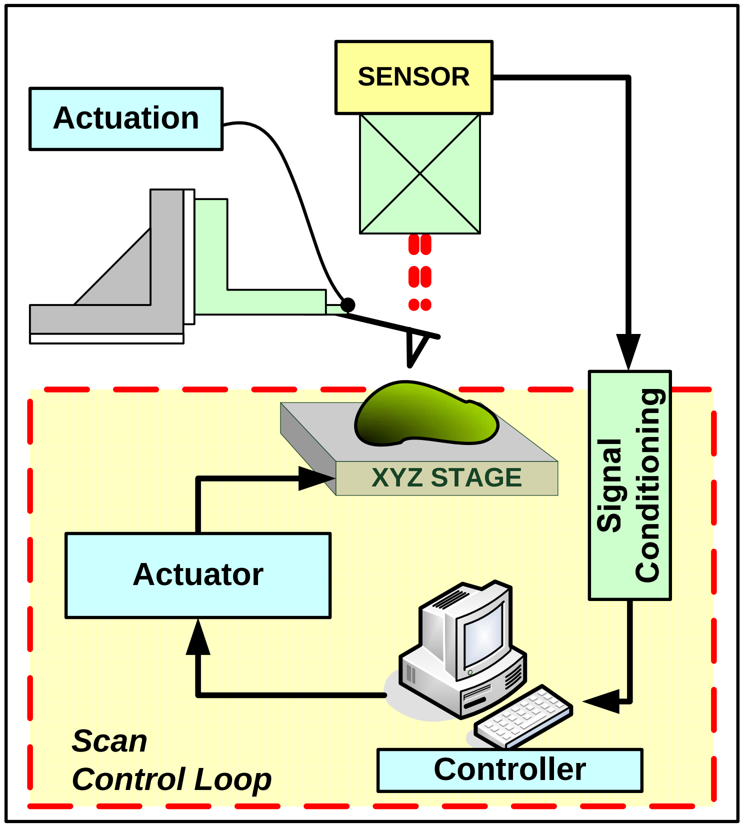

Figure 2.1: Illustration of a basic tapping-mode AFM setup

2.4 Control of Quality Factor of Microcantilevers

In order to limit the tapping forces, AFM probes with high Q-factor are used. The Q-factor of a probe which is inversely proportional to its inherent damping is a measure of the energy dissipation rate. In other words, the amount of energy can be dissipated from the system during each oscillation cycle is limited by Q. In order to have a probe with high Q-factor, either the physical dimensions of the probe has been reduced or the probe is operated in vacuum where the air damping is insignificant. Using a probe with high Q-factor has shown to reduce the magnitude of the tapping forces (Anczykowski et. al. [8]).

However, AFM probes with high Q-factor dissipate less energy at each oscillation; therefore their response is slower compared to the probes with low Q-factor. On the other hand, the dynamic response of a probe with high Q-factor is slow and results in a decrease in maximum achievable scan speed.

In order to change the effective Q-factor of a probe actively, Q-control is introduced [9]. The effective Q-factor of a cantilever probe can be set to a desired value prior to scanning by means of an extra circuit, including a phase shifter and a gain amplifier, in the feedback loop. The measured displacement signal of the probe is phase shifted and added to the actuation signal after scaled by a constant gain. A detailed theoretical analysis of Q-control and its effect on cantilever dynamics are provided by Rodriguez and Garcia [6]. These theoretical results are extended by Holscher et al. [10] to include the tip-sample interactions based on nonlinear effects. The effect of controlling Q-factor on the sensitivity of oscillation amplitude and phase signal is investigated by Kokavecz et al.[11]. Increasing the sensitivity of the probe using a phase shifter without affecting the oscillation amplitude is also suggested in [12]. The imaging bandwidth of tapping-mode AFM probes under Q-control is analyzed in [13]. Sulchek et al. [9, 14] showed that the sensing bandwidth of a probe and the scan speed can be improved significantly by actively lowering the Q-factor of the probe. However, increased energy dissipation at each oscillation cycle causes the tip to tap harder onto the sample. Hence, there is a trade-off between the scanning bandwidth and the tapping forces in setting the effective Q-factor of an AFM probe. This trade-off is more emphasized when imaging soft biological samples in liquid [15, 16, and 17]. While the Q-factor of the probe is naturally reduced due to high viscous damping in liquid which allows faster imaging of biological samples in their native environment, the large tapping forces may cause damage on the sample.

Chapter 3

THEORY

3.1 Introduction

In this section, mathematical modeling of a simple cantilever probe is presented. The sub-sections are thus devoted to the modeling of the cantilever, to the study of the interaction forces between the probe tip and the sample in tapping mode AFM operation and the modeling of the probe dynamics focusing on the theory of quality control.

3.2 Mathematical Modeling of AFM Probe

The AFM probe is a distributed parameter system; hence a good model can be achieved using Partial Differential Equations (PDEs). However, since PDEs yield very complex models for analysis and controller synthesis, Ordinary Differential Equation (ODE) based models are much more useful and they are more common in the literature. The PDE for a freely vibrating micro-cantilever is as follows [18],

$$EI\frac{\partial^4 z(\xi,t)}{\partial \xi^4}+m\frac{\partial^2 z(\xi,t)}{\partial t^2}=0 \qquad (3.1)$$

where ξ is the normalized position, t is the time, EI is the flexural stiffness, m is the constant mass per unit length. In case of tip-surface interaction forces the equation can be written as,

$$EI\frac{\partial^4 z(\xi,t)}{\partial \xi^4} + m\frac{\partial^2 z(\xi,t)}{\partial t^2} = F(\xi,t) \tag{3.2}$$

where F is the tip-sample interaction force which will be explained in detail in the next subsection. Since the PDEs are infinite-dimensional systems they can be converted to an ODE with infinite number of states using the well-known Modal Analysis approach. This approach is used in [18] to obtain an ODE from the beam equation and this ODE was analyzed in order to determine the characteristics of AFM probe upon scanning. A much more detailed modal analysis approach is given in [19]. Using the modal analysis approach, the higher modes of the system can be disregarded and an ODE of order 2, 4, 6, or 8 can be obtained with great accuracy [18]. If the modal analysis is applied to obtain a second order ODE of the system, we obtain

$$m\ddot{z} + kz + \frac{m\omega_0}{Q}\dot{z} = F_{ts} + F_0\cos(\omega t) \tag{3.1}$$

where m is the point mass, k is the spring constant, and ω_0 is the natural frequency. Finally Q is the quality factor of the probe, F_{ts}, the tip-surface interaction force, and $F_0 cos(\omega t)$ *is* the external driving force acted on the cantilever probe using the piezo-actuators. If there is no tip-surface interaction force, equation (3.1) is basically the equation of a forced harmonic oscillator. Note that without the forces the model is an LTI model. However the nonlinear interaction forces yield a nonlinear negative feedback to the system where the input is a sinusoidal signal. This can be seen better rewriting the equation as follows,

$$\underbrace{m\ddot{z} + kz + \frac{m\omega_0}{Q}\dot{z}}_{LTI} - \underbrace{F_{ts}}_{forces} = \underbrace{F_0 \cos(\omega t)}_{input} \tag{3.2}$$

Although the analytical solution for no interaction forces can be obtained easily (the system becomes an LTI system driven with a sinusoidal signal), obtaining an analytical solution by considering the tip-sample forces is still an active research area. Under the assumption of sinusoidal oscillation, a solution is given by Wang [19, 21]. A different approach was followed by San Paulo and Garcia [22] to find an analytical solution applying the viral theorem. The steady-state solution has been presented in [23] and [24]. A theoretical analysis of the equation from a control point of view is given in [18]. A detailed analysis of the equation using the Melnikov method is also given in [25]. Numerical solution of the equation is also available in the literature [5].

3.3 Modeling of Tip-Sample Interaction Forces

Assuming that the probe is tapping on the surface with a very sharp tip having a spherical shape at the end; interaction forces between the tip and the sample surface are modeled as the interactions of a sphere with an elastic spherical micro-substance. According to the tip-sample separation distance, there are two groups of forces coming into consideration, which are “Non-Contact Forces” and “Contact Forces”.

3.3.1 Non-Contact Forces

Non-Contact Forces are described as the forces acting in the attractive regime, where the tip-sample separation is larger than the interatomic distance of ~0.35nm [26]. Van der Waals forces, capillary forces and the electrostatic forces are considered as the non-contact forces and they tend to shorten the tip-sample separation distance.

Van der Waals Forces

Van der Waals (VDW) forces F_{VDW} are always present while surfaces are interacting. They originate from Lennard-Jones force F_{LJ} which is in the form of

$$F_{lJ}(h) = -\frac{A}{h^7} + \frac{B}{h^{13}} \tag{3.3}$$

The difference between Lennard- Jones forces and van der Waals Forces is that Lennard-Jones forces are between two atoms where van der Waals Forces apply for two particles. In other words, van der Waals forces are the sum of Lennard-Jones forces between two individual atoms of two separate particles. Van der Waals Forces' magnitude depends on the geometry of the contact, the distance, and the interacting materials via the Hamaker constant. For two interacting spheres with radii R_A and R_B Van der Waals Force can be calculated as

$$F_{VDW}(h) = \frac{HR}{6h^2} \tag{3.4}$$

where, H is the Hamaker constant, R the effective radius and h is the distance between surfaces of the objects. The Hamaker constant of the interface between objects A and B can be calculated as

$$H_{AB} = \sqrt{H_A H_B} \tag{3.5}$$

Hamaker constants of several materials are given in Table 3.1.

Table 3.1: Hamaker constants of several materials [27].
(Note that all values are given in Joules x 10^{-20})

Material	Hamaker Constant	Material	Hamaker Constant
Au	45.5	SiO_2	8.55-50
Ag	40.0	Quartz	5.5-42.3
Cu	28.4	Carbon	21.7
Si	25.6	Diamond	28.4
Fe	21.2	PMMA	6.3

Capillary Forces

In wet environments (humidity > 9%) water intervenes in the interfaces of the two interacting objects and cause capillary forces [28]. This force can be calculated as

$$F_{cap}(h) = 4\pi\gamma_L R(1 - \frac{(h-2e)}{2r_1}) \qquad (3.6)$$

where, r_1, e, γ_L and R are the radius of curvature of the meniscus, the thickness of the liquid layer, water surface energy, and the effective radius respectively.

Electrostatic Forces

If the interacting objects are not free of charge, electro static forces are present due to electro static interactions of the objects [28]. This force can be calculated as

$$F_{el}(h) = \frac{\varepsilon_0 U^2 S}{2h^2}, \quad (h>a_0) \qquad (3.7)$$

where ϕ_1 and ϕ_2 are work functions of two surfaces, e_c = 1.6 x 10^{-19} C is the electron charge, S is the contact area, a_0 is the interatomic distance, ε_0 is the permittivity and U equals to $\frac{(\phi_1 - \phi_2)}{e_c}$.

3.3.2 Contact Forces

In the repulsive regime the distance between the tip and the sample surface is <0.35nm (interatomic distance) and contact with the sample and the tip occurs. Resulting forces are calculated using the contact mechanics [29]. Several models for contact mechanics are proposed in the literature.

The Lennard-Jones interaction was first introduced by Muller et al. [30]. This approach models the interaction force upon contact quite accurately. A commonly used model in the literature is the Derjagurin-Müller-Toporov (DMT) model [31]. In DMT model, the tip-sample geometry remains Hertzian but the surface forces are allowed [32]. Another model is given by Johnson et al. [33] known as Johnson-Kendall-Roberts-Sperling (JKRS) model [33, 34]. In this model no force exists between the sample surface and the probe tip if there is no contact, but infinite stress occurs upon contact of these two.

Hertzian mechanics describes the contact conditions better for high loads and low surface forces. For this reason, it is not appropriate for most of the AFM experiments. The DMT theory is the best for rigid systems with small radius of curvature and low adhesion, but this approach can not accurately model the true contact area. Although the JKRS model may yield very low surface forces, it works very well for compliant materials, with high adhesion and small radius of curvature. To the authors' experience and knowledge, the DMT model is generally more suited to the AFM experiments and it is more commonly used.

More recently Maugis [35] and Maugis and Gauthier-Manuel [36] have introduced a transition model from DMT to JKRS based on the Dugdale theory [37]. Using this theory the AFM operation in air was modeled more accurately in [32]. This transition theory was also applied to many other cases for modeling atomic scale forces (see [38] for a recent example). An excellent recent review of the literature is given in [39] for adhesion of soft solids and their contact mechanics.

In this study, DMT interaction model is used to model contact forces and Van der Waals interaction forces are considered as the dominant forces active in the attractive regime. The tip-sample interaction forces are then given as,

$$F_{ts}(z) = \begin{cases} -\dfrac{HR}{6(z_s - z)^2} & , z_s - z \geq a_0 \\ -\dfrac{HR}{6{a_0}^2} + \dfrac{4}{3}E^*\sqrt{R}(z_s - z + a_0)^{3/2} & , z_s - z < a_0 \end{cases} \tag{3.8}$$

where, z is the tip deflection towards the sample, z_s is the distance between the sample and the tip of the undeflected cantilever, H is the Hamaker constant, R is the tip radius, a_0 is the inter-atomic distance, and E^* is the effective contact stiffness given by,

$$\frac{1}{E^*} = \frac{1-{\upsilon_t}^2}{E_t} + \frac{1-{\upsilon_s}^2}{E_s} \tag{3.9}$$

with E_t and E_s being the elastic moduli and v_t and v_s being the Poisson ratios of the tip and the sample respectively.

3.4 Theory of Q Control

In this section, the definition of Q-factor will be introduced and its relation with a vibrating cantilever probe will be investigated. The theory of Q-control will be introduced with equations describing this control method. The quality factor Q of a vibrating system is defined in many ways:

- Q-factor of a vibrating system is a measure of the energy dissipation rate. The amount of energy can be added or dissipated from the system during each oscillation cycle is limited by Q and it is inversely proportional to damping term. In a basic spring mass damper system (like Eq.3.2), this relation is expressed as

$$b = \frac{m\omega_0}{Q}. \tag{3.10}$$

- Q is the number of oscillations at which the vibrating systems response decreases 3dB after the driving force is set to zero.
- Q is the ratio of damped resonance frequency ω_R to -3dB bandwidth or FWHM (Full Width at Half Maximum) bandwidth

$$Q = \frac{\omega_R}{\omega_{FWHM}}. \tag{3.11}$$

- Q of a vibrating system is related to the response time T of the system and damped resonance frequency ω_R as

$$T = \frac{\omega_R}{Q}. \tag{3.12}$$

- Q is the ratio of a vibrating systems response at resonance to the corresponding DC response.

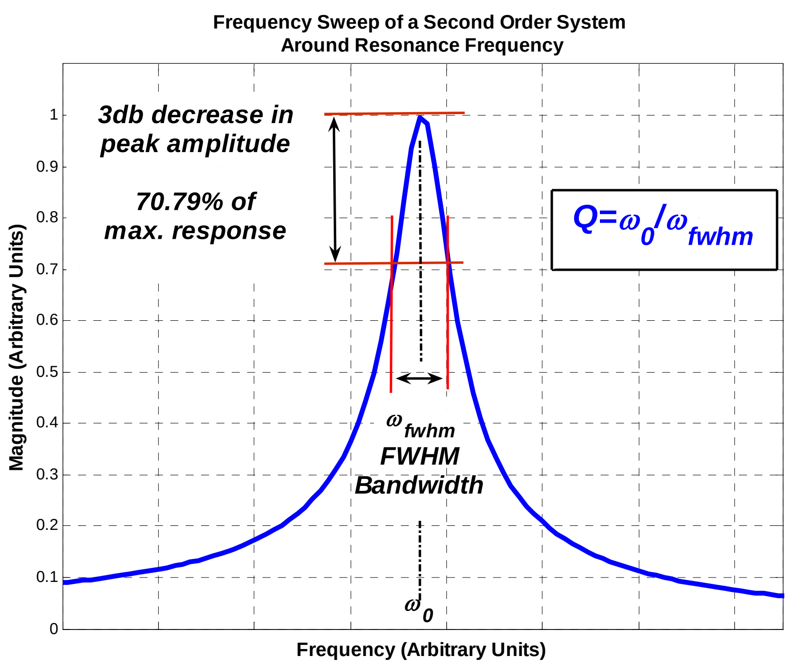

Figure 3.1: Illustration showing how to calculate Q-Factor from a resonance curve. At high Q values $\omega_R \approx \omega_0$

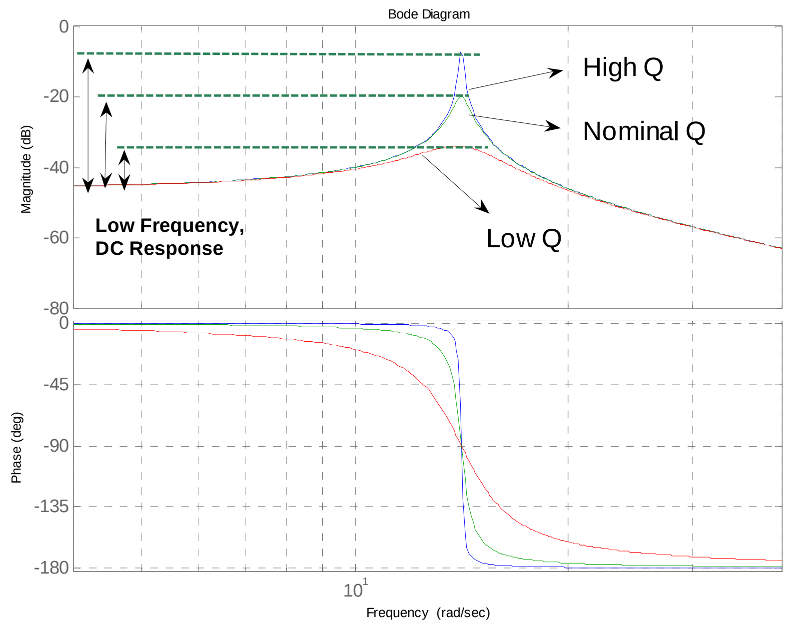

Figure 3.2: The relationship between Q-Factor and frequency response

The above relations show that Q-factor of a probe gives vital information describing its dynamics and limits of operation. These relations imply that,

1. AFM probes with higher Q values dissipate or gain less energy at each oscillation, therefore their response is slower compared to the probes with low Q values. In other words, one can scan faster and take faster AFM images using a probe with low Q value.
2. Higher damping and increased energy dissipation at each oscillation cycle causes the tip to tap harder onto the sample during scanning. The average tip-sample forces are shown to be [4, 6]

$$\langle F_{ts} \rangle = \frac{k}{Q_{eff}} \left[A_0^{\,2} - A_{sp}^{\,2} \right]^{1/2} \tag{3.13}$$

where, A_0 is the free air vibration amplitude and A_{sp} is the set amplitude during tapping mode scanning.

Q-control is introduced by [9] to change the effective quality factor of a micro-cantilever in order to achieve desired dynamical response. Assuming the AFM probe as a spring mass damper system (second order ODE as in Eq.3.1), the equation of motion of can be rewritten as.

$$\left.\begin{aligned} & m\ddot{z} + b\dot{z} + kz = F_{ts} + F_o \cos(\omega t) \\ & \omega_0 = \sqrt{\frac{k}{m}} \\ & Q = \frac{m\omega_o}{b} \end{aligned}\right\} \tag{3.14}$$

where, ω_0 is the natural frequency. The main idea behind Q-control is to modify the damping coefficient b of the cantilever by adding a feedback signal to the actuation signal as given in Eq.3.15, where G and H determine the amount of velocity and position feedback respectively.

$$m\ddot{z} + b\dot{z} + kz = F_{ts} + F_o \cos(\omega t) + G\dot{z} + Hz \tag{3.15}$$

$$m\ddot{z} + (b - G)\dot{z} + (k - H)z = F_{ts} + F_o \cos(\omega t) \tag{3.16}$$

$$\left.\begin{aligned} & m\ddot{z} + \frac{m\omega*_0}{Q*}\dot{z} + kz = F_{ts} + F_o\cos(\omega t) \\ & \omega_0^* = \sqrt{\frac{m}{(k-H)}} \\ & Q^* = \frac{m\omega_0^*}{(b-G)} \end{aligned}\right\} \tag{3.17}$$

Eq.3.15 to 3.17 indicate that pure velocity feedback only modifies the Q factor of the system whereas any position feedback leads to both modification of Q and natural frequency ω_0. In most of the AFM setups, cantilever motion is measured using photo detectors, which actually sense the vertical (z) position of the probe. Moreover, phase shifters are used to make the transition from z to $\dot{z}$ since position and velocity signals have 90˚ phase shift between each other. The artificial phase shift added to the measured position signal defines the amount of velocity and position components in the feedback signal, which actually determine the resulting value of Q and natural frequency ω_0 of the cantilever.

In the following part two cases will be considered when analyzing the dynamics of the Q-control process. First, the tip-sample interaction forces are neglected and the analytical solution of the Eq. 3.1 will be presented. Then, the contribution of tip-sample interaction forces will be discussed. The latter situation has been analyzed in very few studies recently and an analytical solution does not exist yet.

When the tip-sample forces are not present, the equation governing the cantilever dynamics with Q-control feedback becomes [6],

$$\ddot{z}(t) + \frac{\omega_0}{Q}\dot{z}(t) + {\omega_0}^2 z(t) + \frac{k}{m}gz\left(t - \frac{\phi}{\omega}\right) = \frac{F_0}{m}\cos(\omega t) \tag{3.18}$$

In this equation, g is the Q-control gain and ϕ is the phase shift. Equation 3.18 is equation can be rewritten as,

$$m\ddot{z}(t)+\frac{m\omega_0}{Q}\dot{z}(t)+kz(t)+kgz\left(t-\frac{\phi}{\omega}\right)=F_0\cos(\omega t)\,. \qquad (3.19)$$

The analytical solution of this equation can be written as,

$$z(t)=z_h(t)+z_p(t) \qquad (3.20)$$

where, $z_h(t)$ is the homogeneous solution and $z_p(t)$ is the particular solution. The earlier studies [8, 9, 40, 41] do not take the homogeneous solution into account when giving a steady-state solution to $z(t)$ and they consider only the case where $\phi=90°$. The particular solution of the equation is of the form [6],

$$z_p(t)=A(\omega,g,\phi)\cos(\omega t-\varphi(\omega,g,\phi)) \qquad (3.21)$$

where,

$$A(\omega,g,\phi)=\frac{F_0/m}{\sqrt{\left(\omega_0{}^2-\omega^2+\frac{kg\cos\phi}{m}\right)^2+\left(\frac{\omega\omega_0}{Q}-\frac{kg\sin\phi}{m}\right)^2}} \qquad (3.22)$$

with $\phi=90°$ the effective Q-factor can be estimated as [6],

$$\frac{1}{Q_{eff}}=\frac{1}{Q}-\frac{kg}{m\omega\omega_0} \qquad (3.23)$$

A detailed analysis covering the dependence of Q factor and ω_0 on phase shift was published by Rodriguez and Garcia. However the result given by equation (3.23) is shown to be inconsistent with the numerical solutions for higher Q values in [6]. It is further shown that the particular solution underestimates the Q value for $\phi = 90°$ with numerical solution of the equation. For the condition that $\phi = 90°$, the Q-control feedback term becomes,

$$gz\left(t - \frac{\phi}{\omega}\right) = -\frac{g}{\omega}\dot{z}(t) \qquad (3.24)$$

which is a term proportional to the velocity. Then equation (3.18) becomes,

$$\ddot{z}(t) + \frac{\omega_0}{Q}\dot{z}(t) + \omega_0{}^2 z(t) + \frac{k}{\omega m} g\dot{z}(t) = \frac{F_0}{m}\cos(\omega t) \qquad (3.25)$$

which has the analytical solution [6],

$$z(t) = z_h(t) + z_p(t) = e^{-\beta t}(C\cos\varpi t + D\cos\varpi t) + A(\omega)\cos[\omega t - \varphi(\omega)] \qquad (3.26)$$

where,

$$\beta = \frac{\omega_0}{2Q} - \frac{kg}{2m\omega} \qquad (3.27)$$

and

$$\varpi = \omega_0\sqrt{1 - \frac{1}{4}\left(\frac{1}{Q} - \frac{kg}{m\omega_0\omega}\right)^2} \qquad (3.28)$$

As shown in [6], this last equation yields an unstable behavior for (3.8) when,

$$\frac{\omega}{\omega_0} < \left(1 - \frac{Q}{Q_{eff}}\right) \tag{3.29}$$

Note that the unstable behavior is not observed if the driving frequency is equal to the resonance frequency, but if they are different stability issue will be important.

The solution of the ODE for Q-controlled cantilever and the tip-surface interaction was given in the very recent work of Hölscher et al. [10]. Expanding the tip-surface interaction forces using Fourier series and neglecting the higher order terms, Hölscher et al. obtain the same results of [6] but they have further pointed out that,

$$Q_{eff}(g, t_0) = \frac{1}{1/Q_0 - g\sin(2\pi f_d t_0)} \tag{3.30}$$

extending (3.6) of [6] one step further to include the phase shift as well. It was also shown in [10] that for $\phi = 90°$ and $\phi = 270°$ the effective Q-factor can be calculated as,

$$Q_{eff} = \frac{1}{1/Q_0 \mp g} \tag{3.31}$$

where, minus sign is for $\phi = 90°$ and the plus is for $\phi = 270°$. This basically causes an increase or decrease in the effective Q-factor. Note that there will be a limit for changing the resonance frequency. This limit is calculated for a specific cantilever model in [10].

A solution to the ODE governing the dynamics of the probe was also given by [11] They present a solution for steady-state of the equation for freely vibrating cantilever under Q-control using a graphical approach while solving only some of the parameters numerically. In [11] the time to reach the steady-state solution is shown by simulations. They have shown that with Q-control a better contrast in phase images can be seen, but there is a maximum probe sensitivity that can be achieved with Q-control.

Chapter 4

SET-UP

4.1 Introduction

This section summarizes our efforts in constructing a nano scanning set-up for imaging at nano scale. Section 4.2 describes each component used in the set-up and how they are integrated into each other. Section 4.3 introduces the control loop for “Adaptive Q-Control”.

The components of the set-up for nano-scanning setup are shown in Figures 4.1 and 4.3. A sample to be imagined is mounted on a XY raster scanning nano stage. The vibrations of the self-actuated nano probe, which is tapping on to the sample, is measured using a Laser Doppler Vibrometer (Polytec Inc., Germany) mounted on an optical video microscope system. A firewire camera (Point Grey Research Inc., Vancouver) and a light source are used for online visual imaging. The set-up is capable of focusing the laser beam down to a spot size of ~2 μm and positioning the spot on any point in the view area of the microscope using a 10X long working distance optical lens and the laser beam positioner (OFV-71). A signal processing circuit is employed to compute the root mean square (RMS) value of the vibrometer output signal. The circuit also enables the user to actively control the quality factor of the probe during scanning via an xPC Target controller. Using NI DAQ cards the vibration amplitude of the nano-probe is sampled into two computers, one running the scan controller and the other running the adaptive Q-Controller. The scan control loop maintains constant vibration amplitude by moving the nano stage in the Z axis up and down during the raster scanning of the sample and the adaptive Q-controller adjusts the Q-factor of the probe during scanning when necessary.

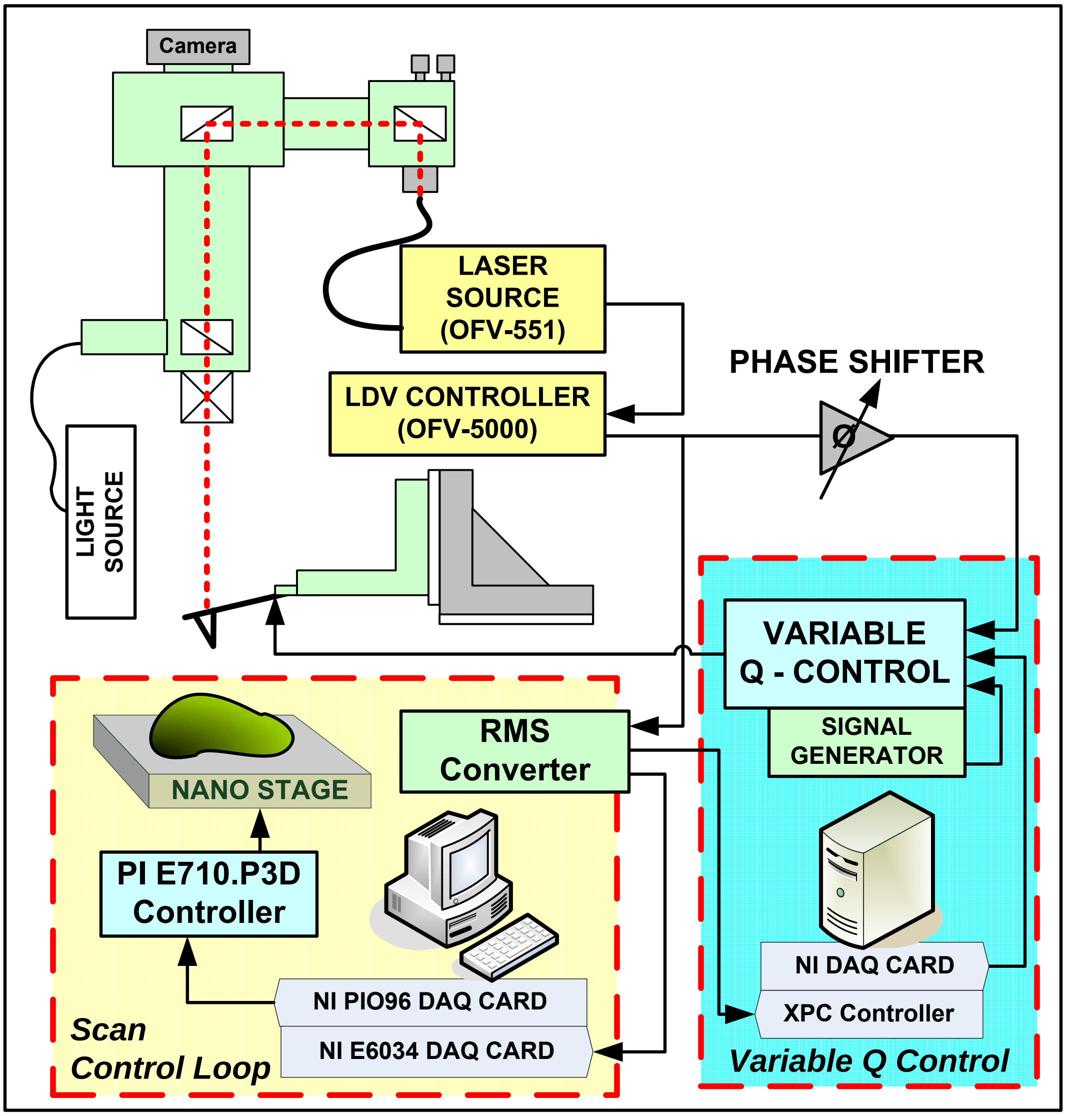

Figure 4.1: Illustration of the AFM set-up utilizing adaptive Q-control.

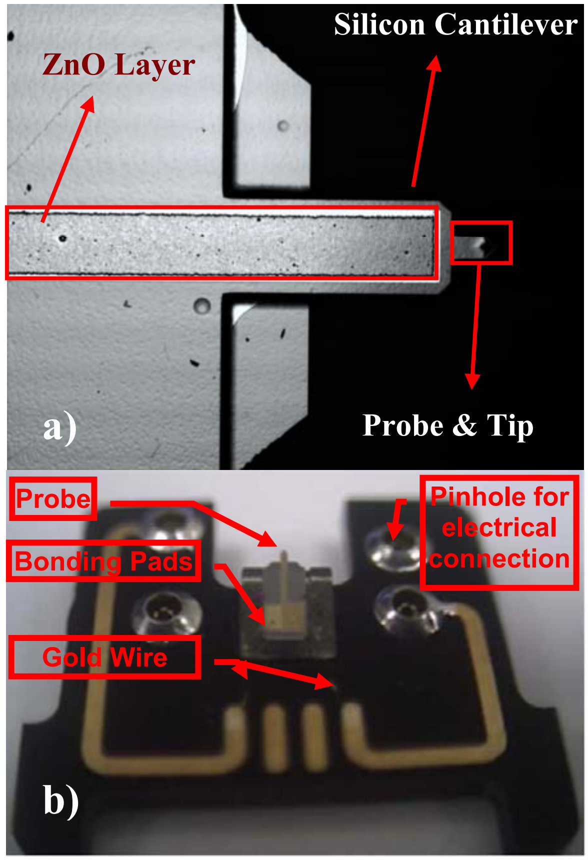

Figure 4.2: Picture of the AFM probe: a) Self actuated bimorph cantilever probe (tip side up). b) The probe is supplied by the manufacturer as glued and wire bonded on a chip

4.2 Parts of the Developed Setup

4.2.1 Probe

A commercially available self-actuated AFM probe (DMASP, Veeco Probes Inc., Santa Barbara, CA) is used for scanning the sample. The probe contains a ZnO stack (consisting of 0.25µm Ti/Au, 3.5µm ZnO, 0.25µm Ti/Au) at its base [42]. This stack, along with the silicon cantilever, acts as a bimorph actuator to control the vertical displacement of the probe tip (Figure 2a). When voltage signals are applied to the pads at the fixed end of the cantilever, the ZnO layer expands or contracts according to the piezoelectric phenomena causing the bimorph probe to bend. In this way, the cantilever can be resonated by applying voltage signals at a desired frequency. The probe which is already glued and wire bonded on a chip (Figure 2b) is mounted on a manual XYZ stage (462 Series, Newport Inc., Germany) to bring it sufficiently close to the sample surface.

4.2.2 Laser Doppler Vibrometer

A Laser Doppler Vibrometer, LDV, (Polytec GmbH, Germany.) is used for measuring the vibrations of the probe. The LDV having a bandwidth of 1.5MHz, measures the out of plane velocity of a point on the probe by collecting and processing the back-scattered laser light. The fiber-optic vibrometer is composed of the vibrometer controller (OFV-5000) and a fiber interferometer (OFV-551). The OFV-551 sensor head has a He-Ne red laser beam source (λ = 633 nm) utilized with a flexible fiber optic cable. The fiber optic cable delivers the laser light to the measurement point and collects the reflected light. Using a microscope system (VM-1V, Meiji Techno Co., Ltd, Japan) with 5X lens the laser beam is focused down to a spot size of ~2 µm. The controller OFV-5000 processes the data collected from OFV-551 using a wide bandwidth velocity decoder (VD-02, which has four output scales (Table 4.1). The measurement data is acquired from the LDV controller (OFV-5000) in scaleable units of mm/s/V. Polytec OFV-71 and OFV-72 units are mounted between the microscope and the CCD camera (Flea, Point Grey Research Inc., Vancouver, Canada) to integrate the microscope system with the OFV-551 of the LDV. OFV-71 contains movable mirrors to deflect the laser beam so that one can manually position the laser spot in the area of view (AOV) of the microscope.

Measurement Scale LDV_{SCALE} (mm/s/V)	Full-scale output (peak to peak) (mm/s/V)	Resolution (µm/s)	Bandwidth (3dB value) (kHz)
5	100	0.8	250
25	500	2	1500
125	5000	5	1500
1000	20000	10	1500

Table 4.1: Characteristics of the vibrometer from the operator’s manual.

4.2.3 Optical Video Microscope

The optical microscope system consists of Meiji–5X objective, VM-1V Video adaptable microscope unit with boom stand, a CCD camera and Meiji FL150 light source with halogen lamp. A field of view of 0.48 mm X 0.36 mm can be achieved with the VM-1V microscope using 1/3” CCD camera with 10X magnification objective. Meiji- S Plan M10X objective is an infinity corrected objective with 0.25 numerical aperture and a work distance of 9.4 mm. The CCD camera is a Point Grey-FLEA CCD 1/3” IEEE-1394 camera with resolution of 1024x768 (pixel size of 4.65µm X 4.65µm). Meiji FL-150 light source is a 150 W halogen lamp used for inline illumination of the view area. An adjustable filter in OFV-72 reduces the intensity of the laser spot going to CCD camera which is helpful when observing mirror-like surfaces.

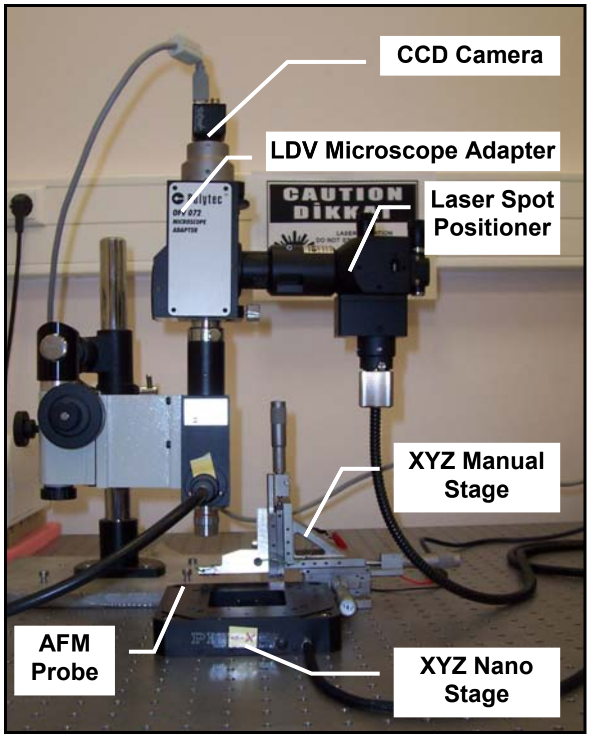

Figure 4.3: Picture of the setup used for nano-scanning.

4.2.4 Signal Processing Circuit

The signal processing circuit consists of a variable phase shifter, an RMS converter, and a voltage multiplier for adaptive Q control. Sub-functional circuit diagrams are shown in Figures 4.4 to 4.6 and the final design is presented in Figure 4.7.

The working principle of tapping mode scanning relies on the detection and control of the vibration amplitude of a scanning probe. The LDV is focused on the nano probe to measure its out of plane vibration velocity using Doppler phenomena. As it will be explained in Chapter 5, due to the time spent during digital signal processing (DSP), there exists a constant time delay between the measured component and the vibrometer output, which results in a phase shift between with constant slope during frequency sweep measurements. The delay circuit (variable phase shifter) in the system eliminates the time delay caused by the DSP of the LDV controller.

The LDV measures only vibration velocity V_{probe} of the nano-probe in volts. Since the control loop requires exact vibration amplitude A_p of the probe, an analog RMS converter (AD536A) is used to make the conversion from V_{probe} to V_{rms}. The relation between V_{probe}, V_{rms} and A_p is given as:

$$V_{rms} = \frac{V_{probe}}{\sqrt{2}} \tag{4.1}$$

$$A_p = \frac{LDV_{scale} \cdot V_{rms} \cdot \sqrt{2}}{2\pi f} \tag{4.2}$$

The conversion between A_p and V_{rms} is computed digitally in the controller. The peak to peak amplitude of the probe is twice the value of A_p.

Phase Shifter

In order to adjust the phase of the measurement signal, a phase shifting circuit (delay circuit) is built. There are several ways to introduce an analog delay into a signal channel. In this work the delay was created using an active circuit (LF351 Opamp). In this approach, a single resistor and capacitor controls the delay line. The Laplace transform of an ideal delay is exponential,

$$\frac{V_O}{V_I} = \exp(-\tau s) \tag{4.3}$$

where t is the desired time delay. The transform (4.3) requires an infinite number of poles and zeroes to implement. Because the ideal form cannot be implemented practically, we use a simple approximation technique known as Padé approximation. The first-order Padé approximation to an ideal delay has the following form (4.4).

$$\frac{V_O}{V_I} = \frac{1 - \tau s/2}{1 + \tau s/2} \tag{4.4}$$

The circuit in Figure 4.4 has the following transfer function same as the first order Padé approximation, with the R*C time constant equaling half the desired delay time (4.5).

$$\frac{V_O}{V_I} = \frac{1 - RCs}{1 + RCs} \tag{4.5}$$

R in the circuit was set using a potentiometer R_{var}. This part enables the user to adjust the phase shift when needed.

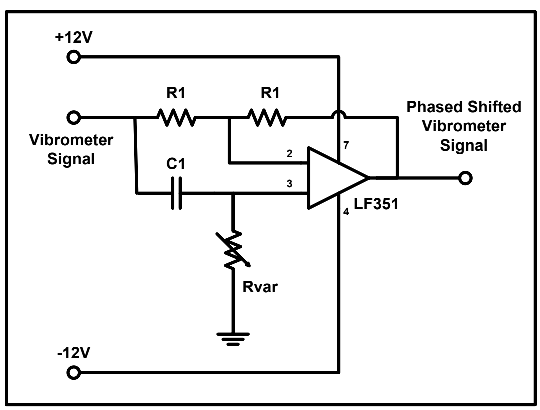

Figure 4.4: The circuit for phase-shifting.

RMS Converter with one pole post filter

In order to obtain the vibration amplitude of the probe from the measured velocity signal in real-time, an analog RMS converter is developed. Since, a nano probe is typically vibrated at or close to its resonant frequencies for better scanning results, the acquisition of complete sinusoidal velocity signal requires high speed sampling. This requirement is eliminated by using an integrated circuit (AD536AJH, Analog Devices, Norwood, MA) which can compute the RMS value of the vibrometer output at update rates higher than the sensing bandwidth of the probe. The capacitor C2 in Figure 4.5 adjusts the width of the running RMS window. Choosing a low value for C2 improves the bandwidth of the RMS converter but increases the ripple in the output. The capacitor C3 acts like a single-pole post-filter increasing the quality of the signal and the bandwidth of the converter.

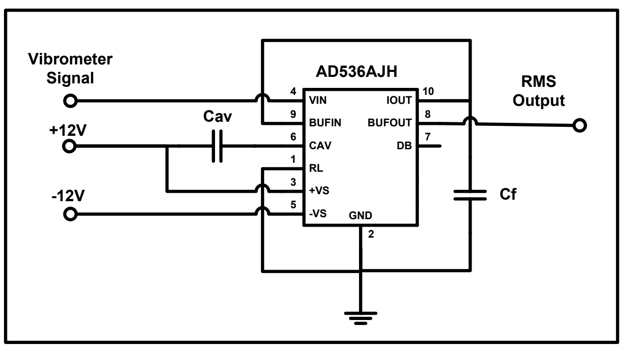

Figure 4.5: RMS to DC converter circuit.

Analog Voltage Multiplier

Analog voltage multiplier circuit enables the system to continuously scale vibrometer signal according to the control signal coming from xPC. Although using a digitally controllable variable resistor or a programmable microprocessor may be alternative solutions for building such a circuit, they have disadvantages. Variable potentiometers are discrete resistors, operating with slow response times. They have limited write up to memory life Moreover, their serial communication with a controller takes valuable processing time which hinders real-time operation. Programmable micro-processors are complex and expensive products.

In our work, analog voltage multiplication circuit is based on an AD633 (Analog Devices) integrated circuit having the transfer function W=[X*Y]/10+Z where, Z is Zcos(ωt) actuation signal from the signal generator at or close to the resonant frequency of the probe, X is phase corrected velocity signal coming from LDV and phase shifter, Y is feedback gain coming from xPC Target and W is the actuation signal sent to the probe for operation under adaptive Q control. Using this circuit (Figure 4.6), measurement signal is scaled proportional to the xPC output.

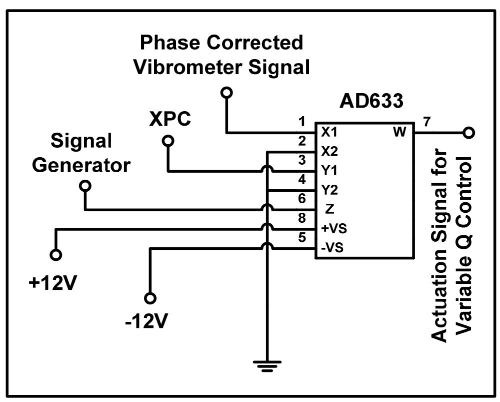

Figure 4.6: Voltage multiplication circuit.

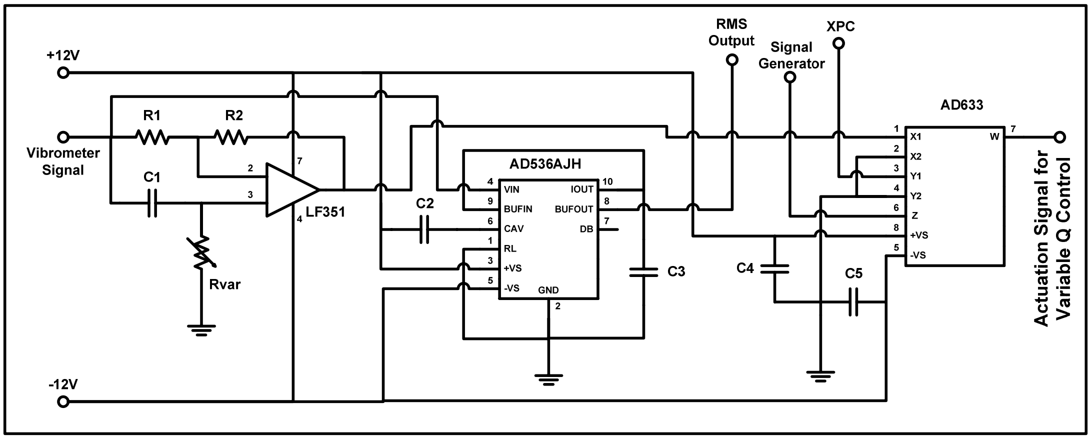

Figure 4.7: The final design of the signal processing circuit.

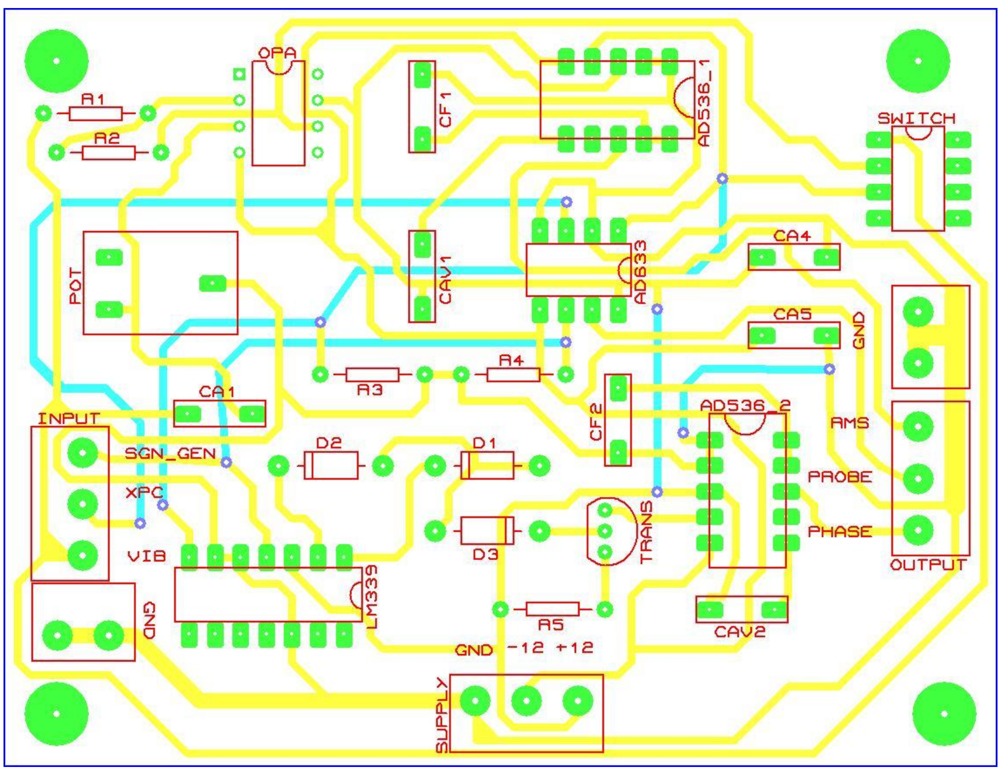

Figure 4.8: PCB print for the signal processing circuit

4.2.5 XYZ Scanning Nano Stage

All movements of the sample surface relative to the probe tip is controlled using a nano-stage (PI Inc, Germany, Model No: P-517.3CD) with a digital controller unit (E-710.P3D). The nano-stage has a travel range of 100 x 100 x 20 µm (nominal resolution is 0.1 nm) and an integrated capacitive sensor for precise positioning. The digital controller of the stage is connected to a digital data acquisition card (NI PCI-DIO-96) via parallel input output port running a high speed servo loop at 0.2ms/cycle. The usage of a digital nano-stage brings high accuracy positioning with velocity controlled motion, noiseless operation, and high accuracy measurement of XYZ position. Moreover, it significantly reduces the non-linearity and creep seen in commercial AFMs during raster scan when a PZT tube is used as the positioning device.

4.2.6 Data Acquisition Hardware

Three DAQ cards are used in the nano-scanning setup. A 96-channel digital input-output card PCI-96 DIO (National Instruments Inc.) is used for the parallel communication with the nano stage. This card is installed into the computer running the scan controller. Using this DAQ card, XY raster scanning and Z controlled movement of the stage is achieved. Communication with the nano stage is achieved using Labview blocks and C/C++ libraries which are provided by the manufacturer of the stage. The second DAQ card PCI-6034E (National Instruments Inc.), which has analog input capability, is used to capture the RMS signal coming from the signal processing circuit. This card is installed into the same computer running the scan controller. 200kS/s sampling rate can be achieved using this DAQ card when using a single channel only. In case of sampling with multiple channels, sampling rate is divided by the number of channels used for sampling. Sampling rate is one of the factors limiting scan speed because the control loop cannot run faster than the sampling time. The third DAQ card is a PCI-6025E (National Instruments Inc.) having analog input and output channels. NI 6025 is installed into a separate PC called xPC. This card runs under Matlab/Simulink and controls the signal input/output for the adaptive Q-Control. Analog input channel 0 (AI0) is connected to RMS output of the signal processing circuit and analog output channel (AO0) is connected to the xPC connector of the signal processing box.

4.2.7 xPC Real-time Target

The xPC target runs a Real-Time Controller which takes the RMS of the cantilever oscillation amplitude as input and controls the feedback gain G of the adaptive Q-control. The software of the xPC embedded computer is built using Matlab/Simulink and converted to C code using the Real-Time-Workshop and Microsoft Visual Studio/Microsoft Visual C++ compiler. The xPC target hardware consists of a high-performance PC equipped with a National Instruments PCI-6025E DAQ card. This PCI card provides connections for to the aforementioned circuits. Phase shifter plus multiplication circuit and an xPC Controller enables the system to continuously control the quality factor of the probe.

4.2.8 Peripherals

In addition to two computers running the scan controller and the adaptive Q controller, one Agilent 33220A 20 MHZ function generator and Agilent DSO3062A oscilloscope are used to generate and observe the input and output signals respectively. Both devices are connected to the host computer using 82357A USB/GPIB interface.

4.2.9 Software

The software interface is developed in Labview (Figures 4.9 and 4.10). Using the interface, the user can easily set all the parameters used in the tapping mode scanning, which are scan speed and scan distance in X and Y directions, the desired tapping amplitude A_{SET}, PID control parameters, and the name and location of the .txt file to record the data.

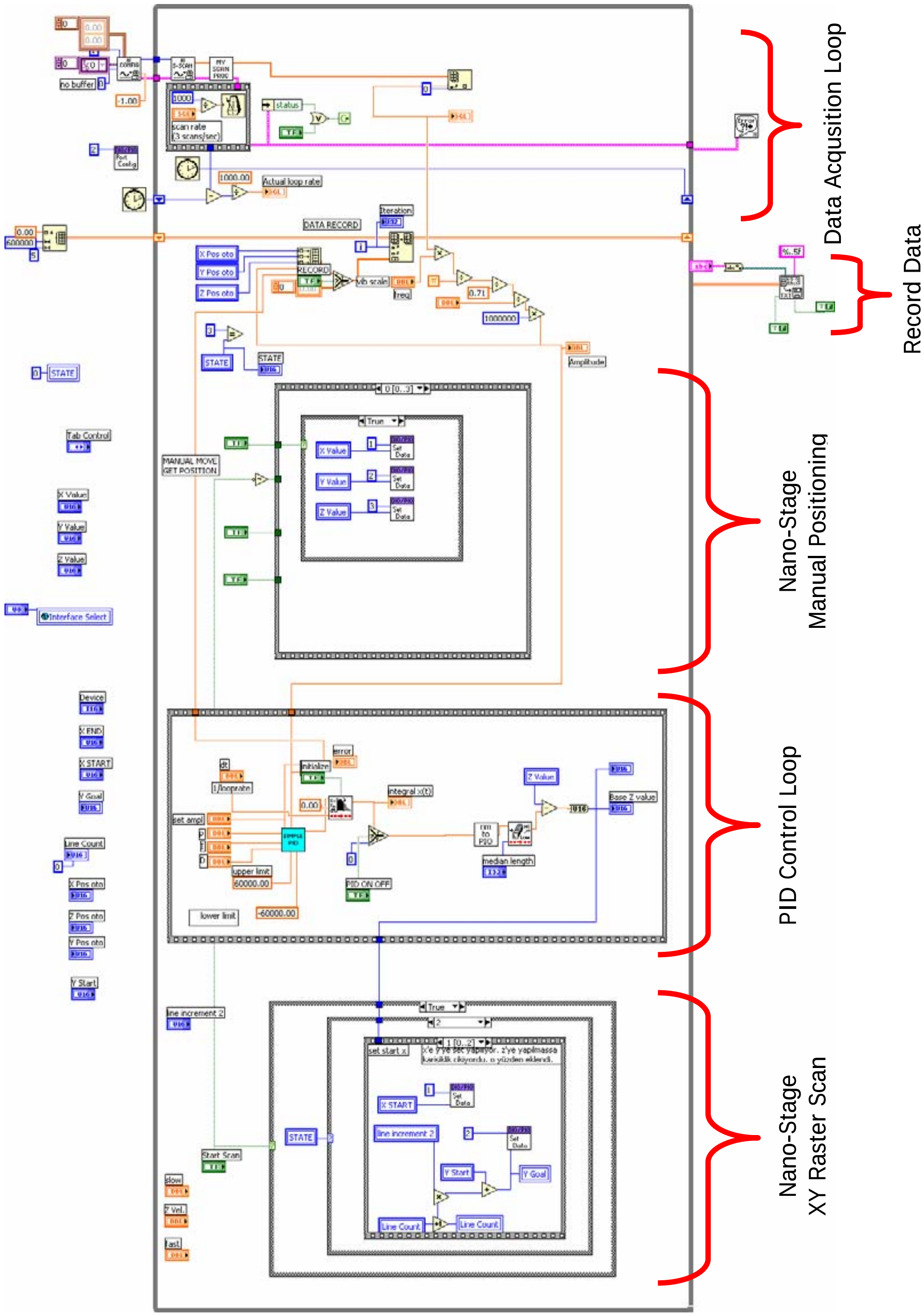

Figure 4.9: The block Diagram of the Labview based scan software.

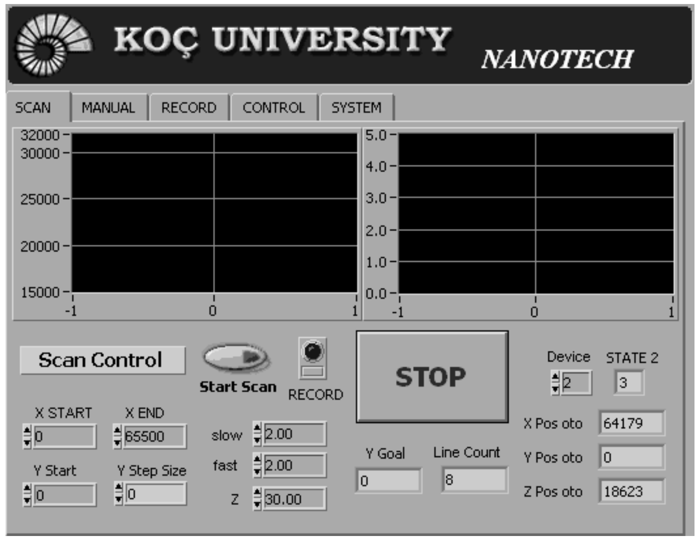

Figure 4.10: The control panel of the Labview based scan software.

4.3 Adaptive Q-Control

In commercial AFM systems, vertical oscillations of the cantilever in the z-direction are measured using a photo detector and a phase shifter is employed to shift the position signal by $\pi/2$ in order to obtain a velocity signal. This velocity is multiplied by a constant gain (G) and added to the actuation signal to modify the Q-factor of the probe. Depending on the application, the value of G is tuned in advance by experience to achieve the desired scanning speeds and the tapping forces. However, there is always a tradeoff between the scanning speeds and the tapping forces. Higher scanning speeds require low Q values which results in excessive tapping forces while light tapping with high Q slows down the scan speed.

The oscillation amplitude A of the probe is limited with the free air amplitude A_0 and during scanning A is controlled to achieve A_{SET}. As mentioned in previous chapters, A_{SET} should be set close to A_0 to avoid excessive tapping forces. When scanning downward steps, cantilever detaches from the surface, vibrates at $A>A_{SET}$ and in the worst case scenario, oscillation amplitude saturates at A_0 causing the error to saturate at A_0-A_{SET}. In cases where A_0 is set very close to A_{SET}, saturated error signal is not large enough to create a fast response for the actuator. Although the tip is detached from the surface and the distance between the tip and the sample is very large, it takes long time to bring A equal to A_{SET} due to error saturation. In [43] this phenomenon is named as “parachuting” and in [14] as “free air error saturation”.

To overcome this problem, we propose the adaptive Q-control. In adaptive Q-control, the Q-factor of the probe is adjusted depending on the surface profile by changing the gain G in real-time as

$$G(t) = G_0 \cdot \left(A - A_{treshold}\right) + G_{set}\,, \qquad \text{(Eq.4.6)}$$

where, G_{set} is a gain value used to set the initial Q-factor of the probe before the scanning starts. When $G_{set} = 0$, the Q-factor of the probe remains unchanged ($Q_{set} = Q_R$, where Q_R is the quality factor at resonance frequency ω_R) unless $A > A_{treshold} > A_{set}$. When the oscillation amplitude A exceeds a certain amplitude threshold A_{set}, the velocity signal is then multiplied by a gain G(t) and added to the actuation signal as in the standard Q-control. This control scheme increases the Q-factor of the system when $A > A_{treshold} > A_{set}$, which in turn increases the free air amplitude and the magnitude of the error signal as well as the magnitude of the control signal sent to the z-actuator. As a result, the system responds faster to the downward steps and the error saturation problem is significantly reduced, leading to faster scanning speeds than the conventional PID controller. The block diagram of the adaptive Q-controller is shown in Figure 4.11 where red and dashed line shows adaptive Q-control loop, blue long dashed line shows the standard Q-control. The block diagram of the adaptive Q-controller generating G(t) is shown in Figure 4.12. This block diagram is developed and compiled using in Matlab/Simulink environment and uploaded into xPC using LAN network.

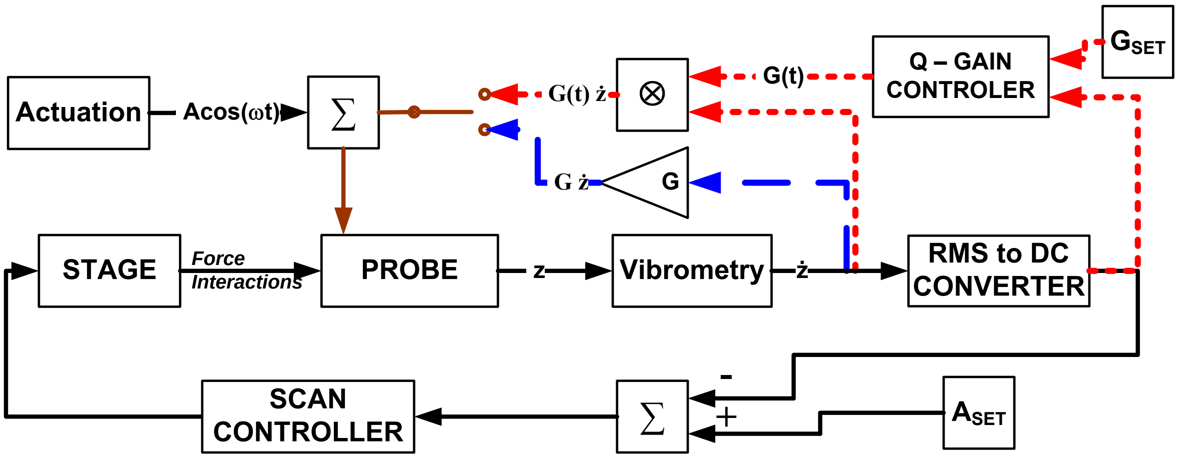

Figure 4.11: Block diagram of the scan controller. Blue long dashed lines show standard Q-control whereas red dashed lines indicate adaptive Q-control.

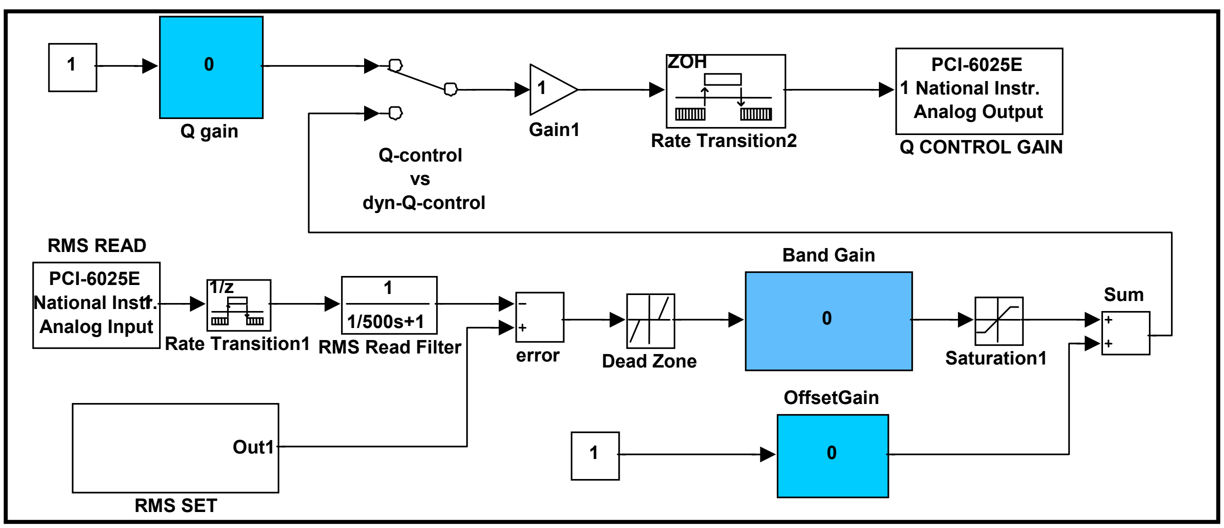

Figure 4.12: Block diagram of the adaptive Q-Control. This Block diagram is developed in Matlab/Simulink and uploaded to an xPC Target.

4.3 Experimental Procedure

- **Turn on the following devices in the given order below:**
    1. Desktop Computer
    2. Signal Generator
    3. Oscilloscope
    4. Laser Vibrometer controller
    5. Fiber Vibrometer (laser source)
    6. Illuminator (light source)
    7. Signal Processing Circuit
    8. Nano-stage Controller

- **Make sure the following cables are connected:**
    1. Signal generator's output channel
    2. Piezo-actuated AFM probe's electrical connection
    3. Synchronization channel between the signal generator and the oscilloscope
    4. Oscilloscope's input channel
    5. DAQ card analog input channel (RMS input to computer)

- **Place the sample** to be scanned on a flat surface (it may be a CD) and put it on the computer controlled nano-stage.

- **Adjust the microscope position vertically and focus the laser pointer on the probe:**
    1. Make sure that 10X lens is used on the microscope.

2. Switch the illuminator on.
3. Place the inclined plane under the microscope so that the laser spot will be perpendicular to the probe surface. This procedure decreases the measurement noise of the laser vibrometer.
4. Position the probe using the micro stage such that the red laser spot points on it.
5. Adjust the microscope position vertically and approach to the probe until you see it on the computer screen. Please first use the coarse caliper of the microscope and then use the fine one. Pay special attention to prevent any collision between the probe holder and the lens while microscope approaches to the probe.

- **Apply the excitation on the probe and measure its vibration velocity:**
  1. Change the impedance settings of the signal generator, and choose "High Z" by following utility -> output setup options on the signal generator's control panel.
  2. Setup the signal such that it's
     a. Amplitude doesn't exceed 300 mV.
     b. Frequency is the third resonance frequency of the probe (you may need to sweep the frequency of the signal and find the frequency that the probe's velocity is the highest. This frequency will be around 210 kHz and it will be slightly different for each probe).
  3. Output the voltage.
  4. Setup the vibrometer controller such that, its scale factor is 25 mm/s/V or 5 mm/s/V.

5. Focus the laser beam on the tip of the probe and observe the measured velocity of the probe on the oscilloscope screen. You should observe a sinus wave on the screen. If you don't, there is a problem and the common sources of the problem are listed below:
    a. There can be contact problem in the cable connections.
    b. The scale of the vibrometer may not be selected correctly.
    c. The supply voltage of the signal processing circuit may not be sufficient.
    d. The laser beam of the vibrometer may not be focused on the probe.
6. If you observe a sinus wave on the oscilloscope screen, then continue with the next step.

- **Bring both the lens and probe to the surface level of the sample and prepare it for scanning:**
    1. Approach to the sample surface by adjusting the vertical positions of both the probe and microscope without losing the view of the probe on the camera. When the distance between the probe and the surface is small enough, move it down slowly and carefully in order to prevent any harm on the probe. You may need to adjust in-plane position of the probe in addition to its vertical position. When the probe tip touches the sample surface, its vibrations will die out and this can be observed on the oscilloscope screen. Also you need to watch the view of the probe captured by the camera while you bring it down to sample surface. The shade of the probe changes when it touches the sample. This is the most important part of the scanning procedure and most unwanted accidents occur in this step. Therefore, pay special attention to your actions in this step.

2. Leave the probe slightly above the surface.
3. Start the “NanoCapture” program and from the “config” menu choose “E 710 Device Interface”. Set the “interface” to “RS232” and “com port” to “com1”. Then click to connect button.
4. After connecting the device, close the “NanoCapture” program.
5. Start the “AFM Scanner” NI Labview program. Make sure that the “NanoCapture” does not run while you start the Labview program.
6. From the “manual” tab, you can control the position of the nano stage manually. Move the nano stage in Z direction upwards until the probe snaps in and the vibrations die out. If you reach the position limits of the nano stage and cannot move it up further, bring it down to its base value in Z and move the probe a little bit down manually. Then repeat the same procedure until the vibrations of the probe die out when the Z position of the nano stage is increased and the vibrations reach to its maximum when the Z position of the stage is decreased.

- **Setup the “AFM Scanner” software for scanning:**
  1. Under the *system* tag:
     i. Input the vibrometer scale and working frequency.
     ii. Read the value in the Amplitude box. This value is the free oscillation amplitude of the probe. Make sure that the probe is not tapping on the sample. If so, move the stage down until the value reaches its maximum.
  2. Under the *control* tag:

i. Input the set amplitude such that it corresponds to 70 % of the free air amplitude. If the probe snaps in frequently, i.e. RMS of the velocity signal is zero; you may want to decrease this value.
ii. Input P value, which the proportional gain in the PID control scheme. The appropriate value P depends on the application and the sample. Therefore you need to find an appropriate P value for the sample by trial and error. High P values cause undesired oscillation of the nano-stage and low P values increase the reaction time and decreases the bandwidth of the scanning system.
iii. Leave I and D values of the PID controller as untouched.

3. Under the *record* tag:
   i. Input the full path of the file in which the data will be recorded for.

4. Under the *scan* tag:
   i. Input the starting and end positions of the scan in X direction.
   ii. Input the starting Y position and positional increment at each line.
   iii. Input the slow and fast Z velocities of the nano-stage.
   iv. Press the Start Scan button.
   v. Start the PID controller by selecting its button under the *control* tag.
   vi. When the nano-stage stops moving in the Z direction, press on the Record button. This starts the recording of the data.

5. Press Stop button when you want to stop the scanning.

Chapter 5

CHARACTERIZATION

5.1 Introduction

In Chapter 3, we showed that a vibrating AFM probe can be modeled as a spring, mass, damper system. In order to characterize the dynamical response of an AFM probe, the spring constant k, damping coefficient b, and mass m must be calculated experimentally. Moreover, the probe used in our set-up is integrated with a ZnO (piezo) bimorph actuator. The conversion from the applied voltage (on the piezo layer) to displacement must be extracted as well. In addition, the scan speed of the system is limited by the slowest component in the set-up. Hence the dynamical response of each part in the set-up must be characterized. This chapter primarily focuses on the characterization of the probe and the signal processing circuit.

5.2 Characterization of the Probe

5.2.1 Static Deflection

In Chapter 4, it was mentioned that the probe used in our system is a self actuated bimorph probe. The term self actuation implies that there is no external actuator to vibrate the probe as in standard AFM systems. When a voltage difference is applied at the electrodes of the bimorph, an electric field generated between two electrodes causes the ZnO film between the electrodes to expand. Since ZnO film, the electrodes, and the silicon cantilever are coupled together, the expansion of the ZnO layer causes the probe to bend one side. Reverse applied voltage results in bending of the cantilever towards the opposite side.

In the first experiment, 1V DC voltage is applied to the probe and the velocity of the tip is measured using vibrometer (See Figure 5.1). The dc deflection of the probe cannot be measured using this method because the transient vibrations (~50kHz at the natural frequency of the probe) dominate the overall measurement. In other words, transient vibrations are much higher than the DC deflection. In order to overcome this problem, a low frequency pulse input ($1V_{peak}$) is applied to the probe. The measured velocity data is filtered using 5kHz low pass filter. The result is shown in Figure 5.2. It is clear that using this method, one can filter the transient vibrations of the probe and extract the velocity component corresponding to the deflection to a 1V DC input. The filtered velocity data is digitally imported to Matlab. The area under the velocity curve shows that the self actuated ZnO bimorph probe deflects 20nm per Volt in low frequencies (DC response).

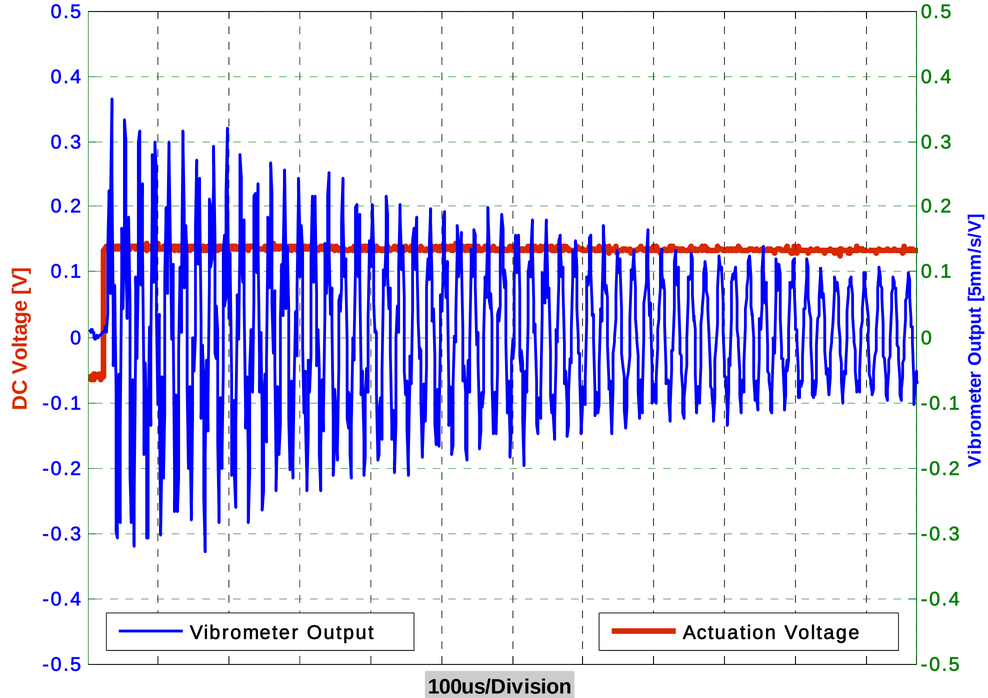

Figure 5.1: Response of the probe to 1V DC input (without filtering)

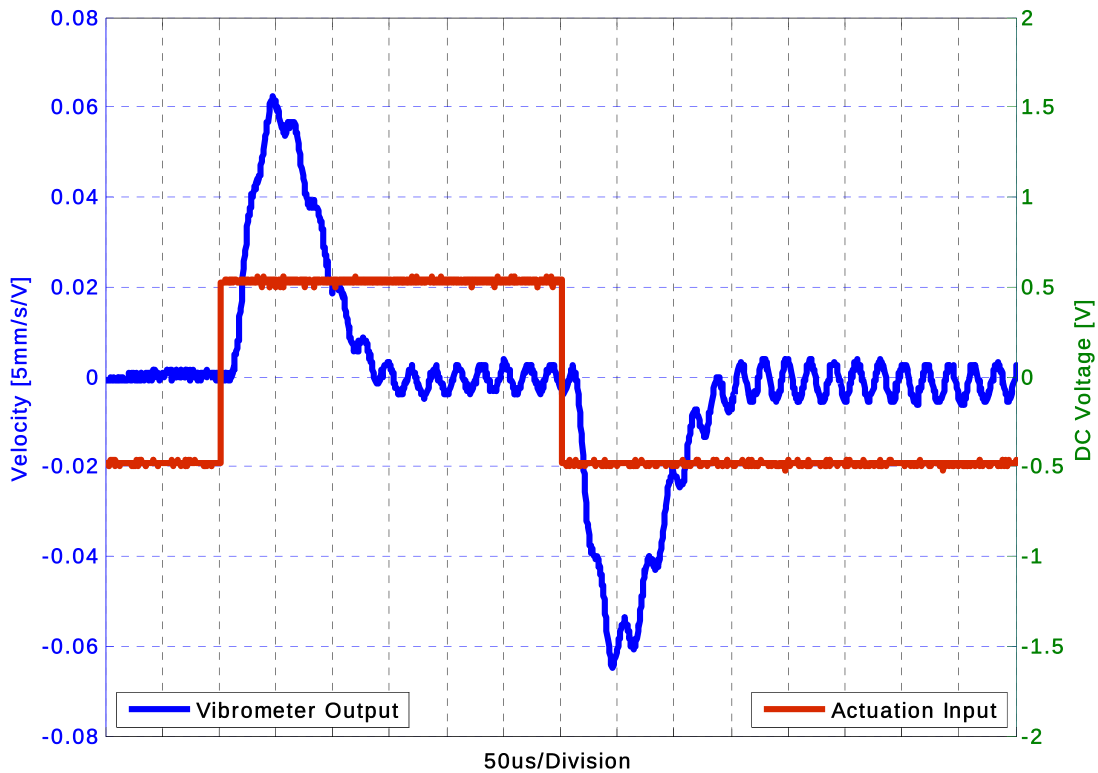

Figure 5.2: Response of the probe to 1V DC input (with 5kHz lowpass filter)

5.2.2 Modal Analysis

Modal analysis is the study of the dynamic properties of structures under vibrational excitation. Using a HP/Agilent 3575A Gain-Phase Meter, response of the probe for different actuation frequencies is recorded (Figure 5.3). Plotting the frequencies in the X axis and the magnitude and phase measurement in the Y axis gives us the Bode plot of the cantilever. The peaks on this frequency sweep plot (in the magnitude graph of the Bode plot) point to resonance frequencies. The curvature (sharpness) of the peaks on this plot is related to the Q factor of the probe. As it was mentioned in Chapter 3, one can calculate the Quality factor of a probe by measuring the FWHM bandwidth of a resonance curve. We fit a polynomial function to the Bode plot of the probe. We used 4th order model because there are only two resonances and each resonance can be modeled as a second order system. In the forthcoming sections, we show how the required parameters are required for each resonance. Blue curve in Figure 5.3 is the measurement data where red curve is the model fitted to the recorded data using “invfreqs” command of Matlab.

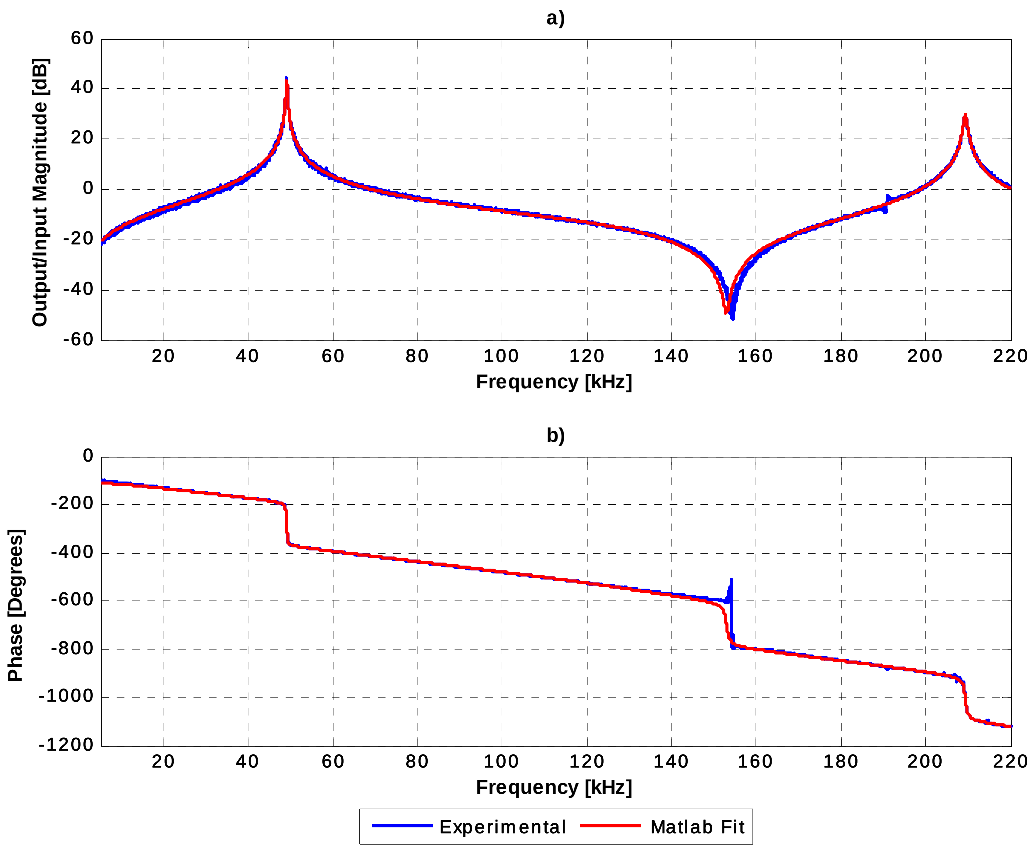

Figure 5.3: Bode plot of self actuated bimorph probe. a) Magnitude curve. b) Phase curve. Blue curve is the measurement data where red curve is the model fitted to the recorded data using “invfreqs” command of Matlab.

Our experiments with LDV showed that there is a constant slope in the phase diagram of the Bode plot (Figure 5.3.b). Figure shows that phase changes linearly with the actuation frequency. Such a phase shift indicates that there is a constant time delay of ~4μs in the measurement system. Further experiments and discussions with the manufacturer of the vibrometer confirmed that the source of this time delay comes is the digital signal processing time spent by the LVD controller.

5.2.3 ANSYS Simulation

Due to its nonrectangular shape, we opted to develop a finite element model of the probe in ANSYS in order to estimate its stiffness, resonance frequencies, and mode shapes via static and modal analyses. We used the material properties of ZnO to model the piezo-actuated movements of the AFM probe. The material properties c11=191, c12=113.2, c13=97, c33=180.2 and c44=38.7 are the elements of the stiffness matrix in GPa, e33=1.28, e31=-0.53 and e35=-0.43 are the elements of the piezoelectric matrix in C/m^2, and e11=6.6 and e33=10.5 are the elements of the permittivity matrix. To construct the geometric model of the probe, width, length, and thickness of the probe are necessary, but it is not easy to measure thickness with a high accuracy. Despite a possible error in geometric model of the probe, the modal analysis of the FEM model matched the real measurements with less than 10% error. Two flexural resonance modes (first and third mode) and one torsional resonance mode (second mode) were observed. The first three mode shapes of the probe obtained using ANSYS are shown in Figure 5.4. Also a static analysis is done in order to get the flexural spring constant of the probe. Static loading divided by the deflection of the load point showed that the probe has a spring constant of approximately k = 14 N/m.

a)	b)	c)
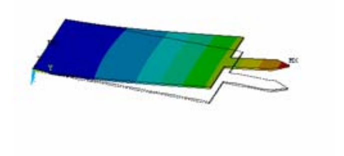	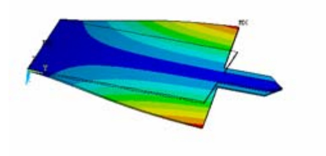	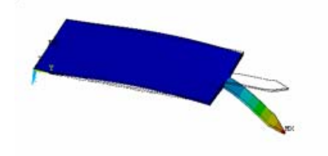
47550 Hz (ANSYS) 48600 Hz (Measurement)	159200 Hz (ANSYS) 155250 Hz (Measurement)	214650 Hz (ANSYS) 208300 Hz (Measurement)

Figure 5.4: Comparison of ANSYS analysis and the experimental results
a) 1^{st} mode shape b) 2^{nd} mode shape c) 3^{rd} mode shape

*Note that experimental values may vary for each probe. In general, it is assumed that probes coming from the same wafer (manufacturing process) have the equal or very close values.

5.2.4 Quality Factor

Detailed information about the Quality factor "Q" is given in Chapter 3. Q is defined as the number of cycles required for the energy to fall off by a factor of 535. (The origin of this obscure numerical factor is $e^{2\pi}$, where e = 2.71828…). The terminology arises from the fact that friction is often considered as an unwanted effect, so a mechanical device that can vibrate for many oscillations before it loses a significant fraction of its energy would be considered a high-quality device. In other words, quality factor "Q" is the number of oscillations required for a system's energy to fall off by a factor of 535 (which equals 3dB drop in the amplitude) due to damping.

Q-factor of the self-actuated bimorph probe is experimentally obtained by plotting the amplitude versus frequency response curve around the resonance frequency and measuring the full width at half maximum (FWHM) bandwidth; ω_R/FWHM gives the quality factor of the corresponding resonance (Table 5.1). Alternatively, this bandwidth can be measured using amplitude modulation method as suggested by [9]. The second resonance mode is a torsional one; hence it cannot be used for scanning in tapping mode. Among the first and third resonance frequencies, the third one is preferred for scanning due to its smaller time constant T, which is related to the Q-factor and the resonance frequency by $T = Q/\omega_R$, where 1/T is defined as the bandwidth. Cantilevers with higher bandwidth enable the scanning system to operate at faster scan speeds.

Mode	**Mode Shape**	**Resonance Frequency (**Hz)	**Quality Factor**	**Bandwidth (**Hz)
1st	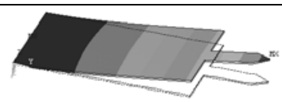	48.600 Hz	129	376
2nd	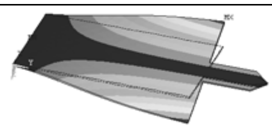	155.250 Hz	-	
3rd		208.300 Hz	332	633

Table 5.1: Quality factor of first three resonances

Although the response of a system at its resonance is Q times larger than its DC response, this does not hold for the piezo actuated bimorph probe. This indicates that the response of ZnO bimorph layers changes with actuation frequency.

5.2.5 Spring Constant

The AFM cantilevers are commonly fabricated from Si, SiN or polymers. Without the cantilevers, atomic force microscopy would not be possible. There are mainly two formulas defining the behavior of the AFM cantilevers. The first one is Stoney's formula, which relates cantilever end deflection δ to the applied stress σ as

$$\delta = \frac{3\delta(1-\nu)}{E}\left(\frac{L}{t}\right)^2 \tag{5.1}$$

where, ν is Poisson's ratio, E is Young's modulus, L is the beam length and t is the cantilever thickness. The second formula relates the cantilever spring constant k to the cantilever dimensions and material constants:

$$k = \frac{F}{\delta} = \frac{Ewt^3}{4L^3} \tag{5.2}$$

where, F is force and w is the cantilever width. The spring constant is related to the cantilever resonant frequency ω_0 by the harmonic oscillator formula

$$\omega_0 = \sqrt{\frac{k}{m}}\ . \tag{5.3}$$

Several methods are proposed in the literature to experimentally calculate the spring constant of a cantilever AFM probe. A detailed comparison of each method is given in [44].

In this study, spring constant of the self actuated bimorph probe is calculated using to Cleveland's Method [45]. In this approach, the spring constant of an AFM probe can be determined by measuring its resonance frequencies before and after adding a small mass on the cantilever. For this purpose, tungsten micro-spheres in different sizes (3 to 10 μm in diameter) are obtained (NT.TG.001, BioForce Nanosciences, Inc., USA). Using a second AFM probe as a manipulator, one tungsten micro-sphere is placed at the very end of the probe close to the tip. The diameter of the placed tungsten sphere is measured under video microscope. Mass of the placed sphere is calculated by multiplying its volume with the density of tungsten (19.25gr/cm^3). Using the Equation 5.3, k is obtained.

Figure 5.5 shows the probe being characterized, the tungsten micro-sphere, and the second AFM probe (V-shaped) used for the manipulation. In this method, the error in the estimation of the tungsten micro sphere affects the estimation of “k”.

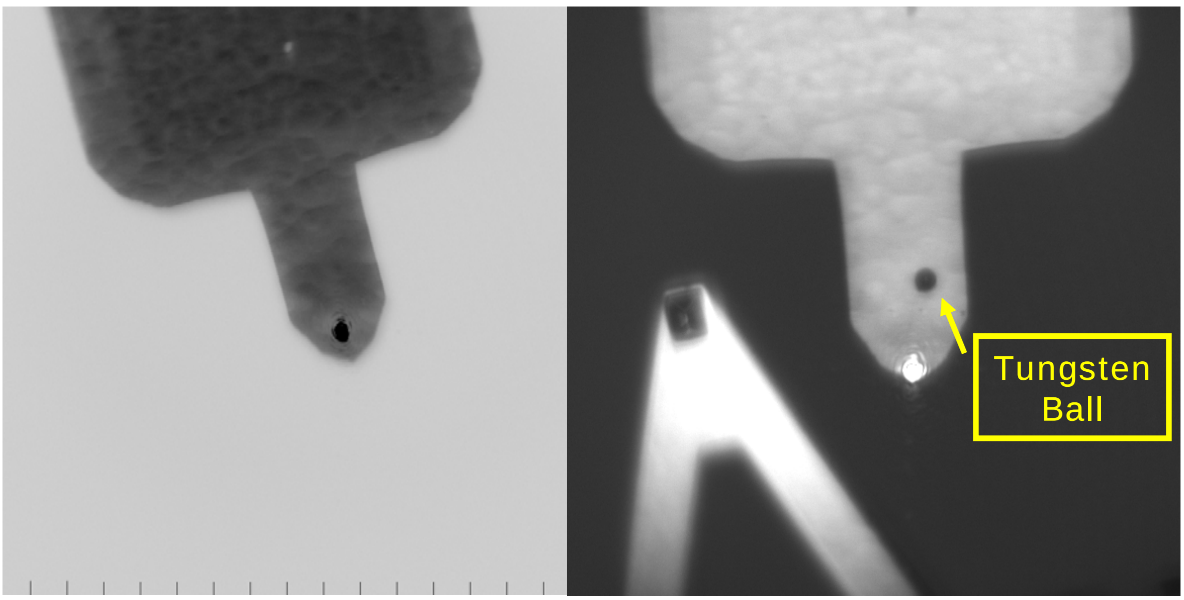

Figure 5.5: Picture of the AFM probe being characterized, tungsten micro-sphere, and the second AFM probe (V-shaped) used for the manipulation.

The optical microscope in our laboratory is equipped with 10X lens which limits the resolution to 0.6μm/pixel. An error in the diameter measurement affects the overall spring constant calculation exponentially. Figure 5.6 shows the results of four experiments conducted by different size tungsten balls. The differences between the measurements are due to the error in determining the exact diameter and hence the mass of the spheres. Using lenses with higher magnification or spheres with known diameter or mass can significantly increase the measurements accuracy.

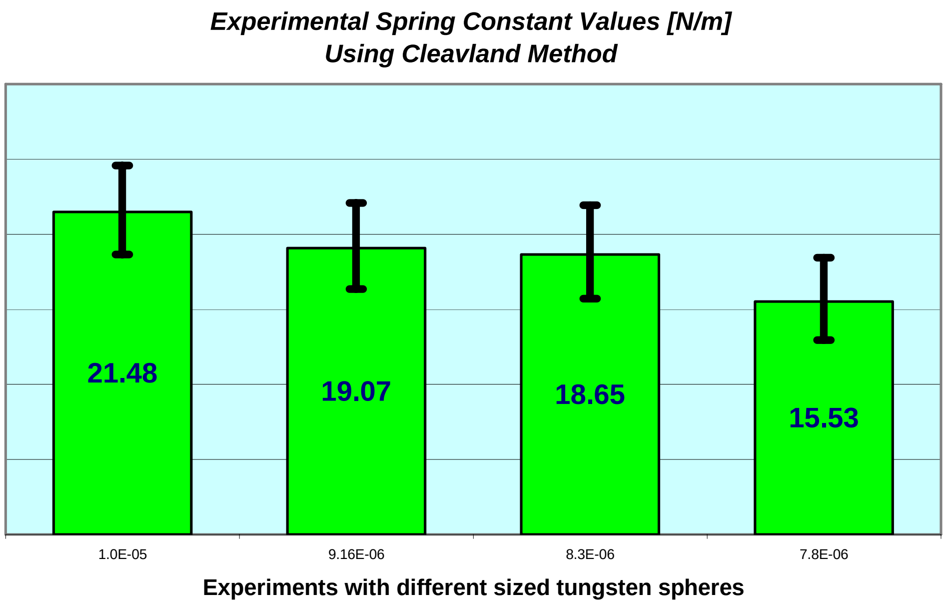

Figure 5.6: The spring constant of the probe is estimated using tungsten micro-spheres.

5.3. Characterization of the Signal Processing Circuit

Probes operating at high resonance frequencies require fast computers and high speed data acquisition systems to record and process the sinusoidal motion completely in real time. Analog RMS to DC converter is employed in our AFM system to make a fast calculation of peak to peak vibration amplitude. It is assumed that a running RMS window covering 10 oscillations of the probe is appropriate. The noise in the output increases as the time constant (width of the running window) of the converter decreases. The bandwidth of the RMS converter should be kept wider than the bandwidth of the probe for proper measurement.

The bandwidth of the RMS converter in our set-up is measured by inputting amplitude modulated (AM) signals at 210kHz and increasing the modulation frequency until 3dB change in the amplitude or in the phase occurs. It is observed that the response of the device to the modulated (AM) input signal is satisfactory up to 5kHz. The effect of phase shift becomes more dominant at increased modulation frequencies. In our set-up, it is sufficient that the conversion bandwidth of the RMS converters must be faster than the response of the probe, which is 600Hz (Figure 5.7) and rises up to 1 to 2 kHz under Q-Control. We should mention that the bandwidth of the RMS converter and the ripple in the output signal affects the quality of scanning. At low signal to noise ratios (especially scanning with low tapping amplitudes) any ripple in the output causes the original RMS signal to get buried under noise. This limits the smallest step size detectable by the probe (Figure 5.8). Moreover, because of the delay in response, forward going and backward going scan lines differ from each other. One pole post filter mentioned above, overcomes these problems and drastically improves the scan performance.

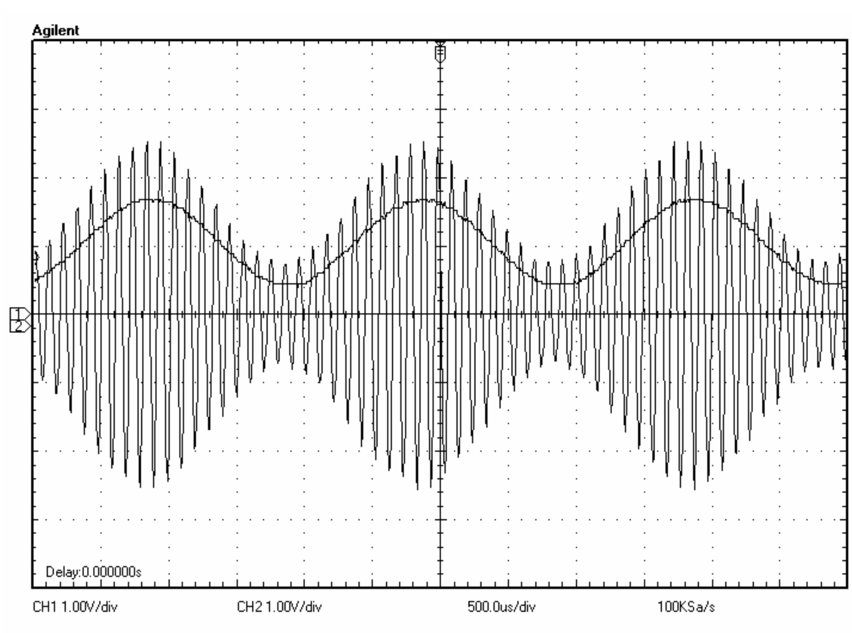

Figure 5.7: Probes response to amplitude modulated signal

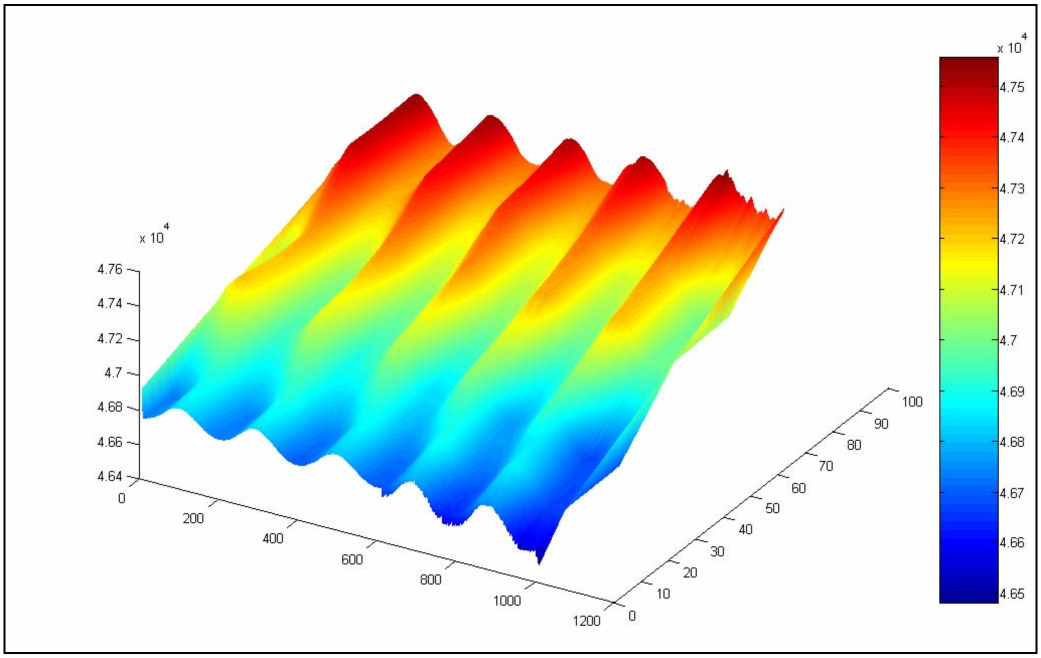

Figure 5.8: Faulty scan due to misadjusted RMS time constant.

5.4. Data Acquisition System and Control Loop

Analog controllers are used in commercial AFM systems to achieve real-time control rates. Due to analog signal processing, controllers can run control loops faster than 40 kHz. Our set-up is based on a digital control loop running on a PC, where data acquisition is done using DAQ cards. The disadvantage of using this combination of hardware is that the resulting control loop can run up to 1 kHz, far slower than the commercial systems. On the other hand, the advantage is that DAQ cards and their development software (Labview, Matlab/Simulink) give us the opportunity to develop different control strategies and test various applications rapidly (rapid prototyping), which was one of the main goals of this study. The main factors limiting the speed of scan control loop are the sampling rate of the DAQ cards and the speed of the internal controller of the stage.

The analog DAQ card used in the scan control loop has a sampling rate of 200KS/s. The scanning control loop has to be run in real time; therefore data must be acquired point by point. Unfortunately, DAQ cards sampling rates drop down to 1KS/s when used in point by point operation. This is the first factor limiting the speed (down to 1ms per loop) of our feedback loop. Moreover, the computer controlled nano-stage has a dedicated controller for positioning, which communicates with the scan control loop using a digital input/output DAQ card. In this case, the limiting factor is that the dedicated controller of the nanostage has an internal control loop updating itself at every 0.2ms. This is the second slowest element in the scan control loop.

As a future work, the nanostage can be replaced with a XYZ piezo tube and an analog controller can be integrated into the system. This replacement will make the scanning process much faster but the movements of the piezo tube along X, Y, and Z axes must be decoupled and the hystresis and nonlinear effects must be considered.

Chapter 6

EXPERIMENTS

6.1 Introduction

In this chapter, images taken with the developed set-up are presented. The first section presents the scan images of the calibration grids using the conventional PID scan-control without Q-control. The second section shows how the quality factor of a probe can be changed actively using the developed signal processing circuit to improve the scan profile. The third section presents the results of the scans obtained using the standard Q-control and the proposed adaptive Q-control. The results show that the adaptive Q-control is superior to the standard Q-control.

6.2 Scanning with Conventional PID

The calibration gratings having periodic steps of 104±2 nm and 20 ± 1 nm (TGZ Series, Mikromash, USA) are scanned using the developed AFM system at different scan speeds and set amplitudes. Scan results show that, the set-up is capable of detecting steps down to 20nm clearly when scan parameters are set properly. The results of the three different scanning methods (without Q-control, the standard Q-control, and the adaptive Q-control) are compared using the calibration grating having step size of 104±2 nm.

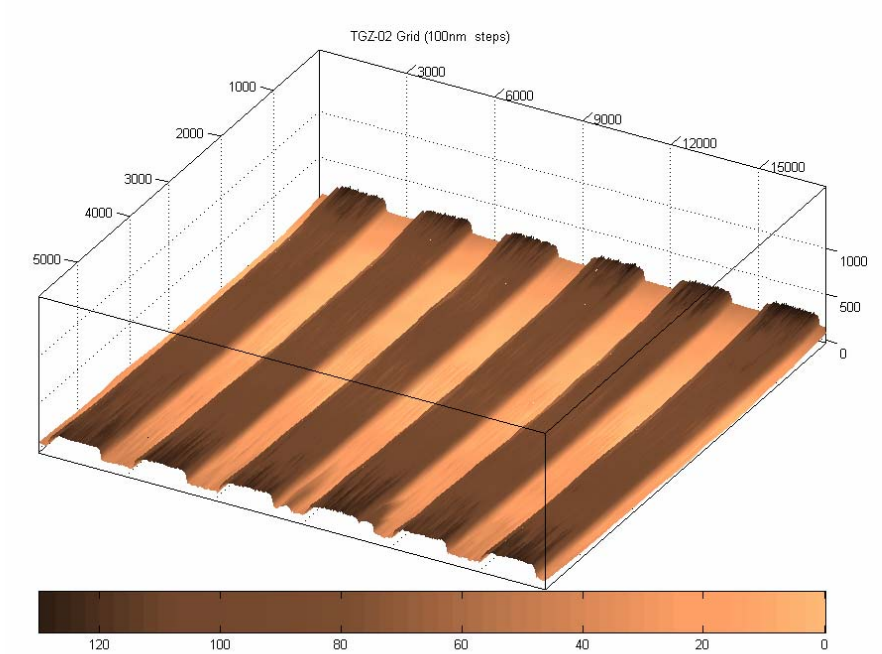

Figure 6.1: Image of the calibration grid with 104nm step height.

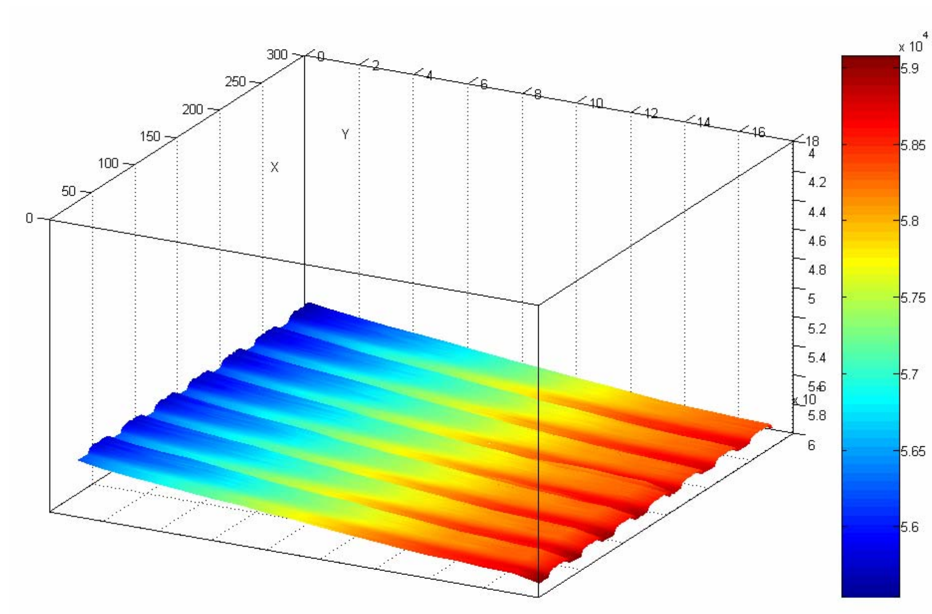

Figure 6.2: Image of the calibration grid with 20nm step height (dimensions are in stage units)

6.3 Active Modification of Q-Factor

The signal processing circuit, which is discussed in Section 3, modifies the effective Q-factor of the bimorph probe in real-time by controlling the value of gain G. The effective Q-factor for different G values is experimentally obtained and shown in Figure 6.1 and it is found that Q-factor increases exponentially as the G value is increased.

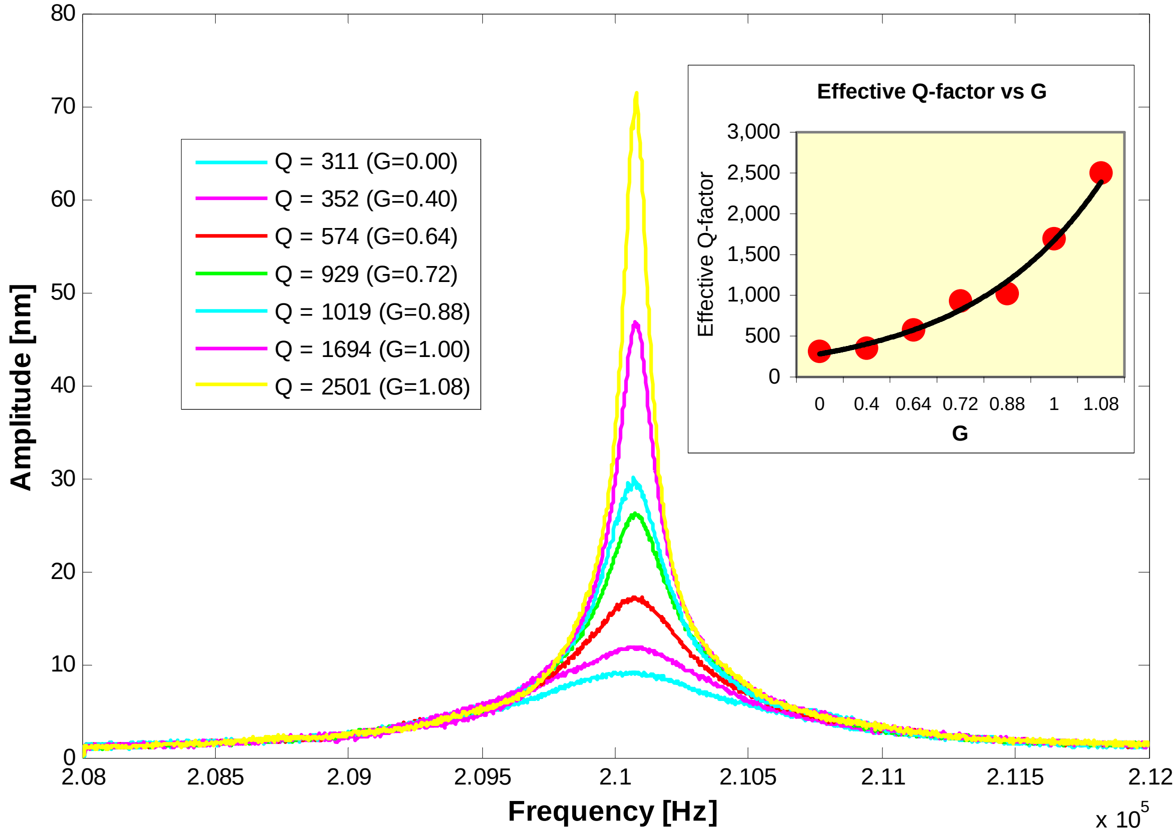

Figure 6.3: Q-factor varies exponentially with the feedback gain G

6.4 Scanning with the Adaptive Q Control

Figure 6.4 and 6.5 show the profile and the error signal of a single scan line for the scan speeds of X and 5X respectively when the standard PI controller is used for scanning (i.e. without Q-control). The slow response of the PI controller at high speeds causes error saturation and an inclined profile for the downward steps (see Figure 6.5). The adverse effects of the error-saturation on the scan profile increases as the scan speed is further increased. This limits the scan speed of the system when the standard PI control is employed.

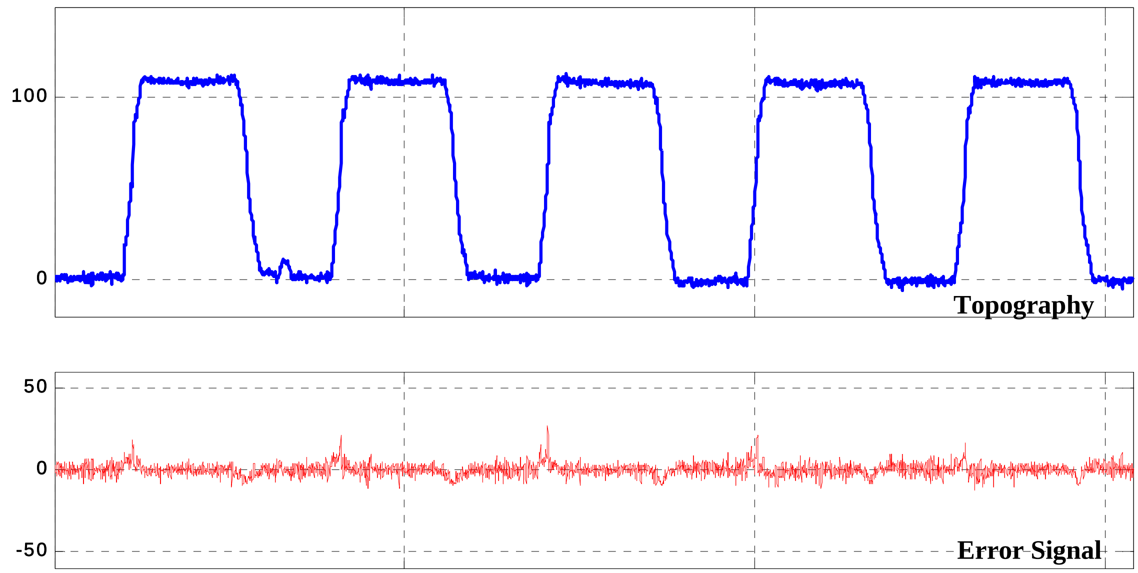

Figure 6.4: The scan profile and the error signal for the scan speed of X (standard PI controller)

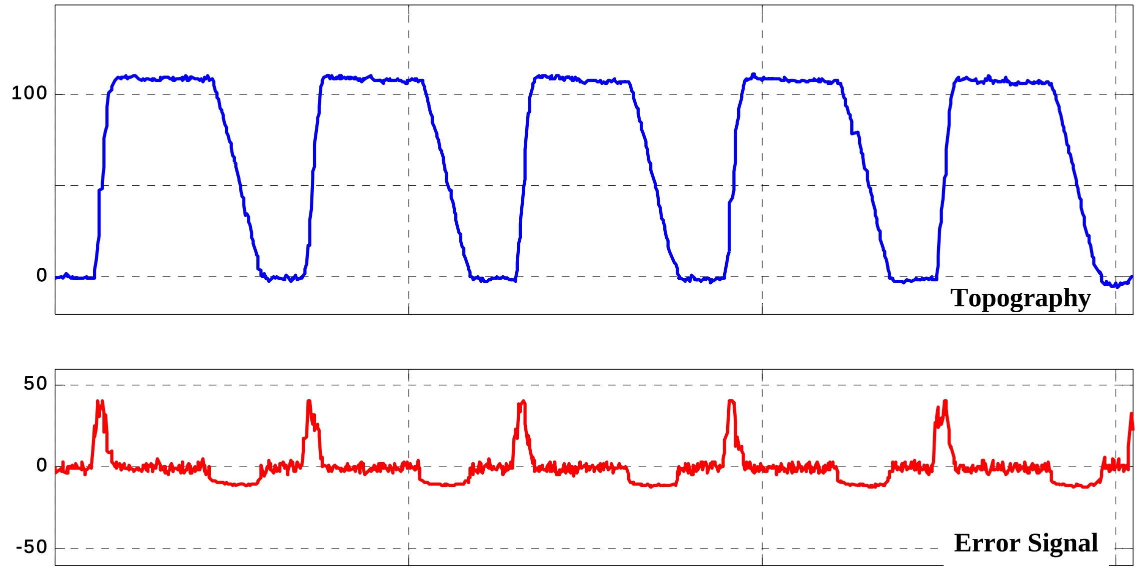

Figure 6.5: The scan profile and the error signal for the scan speed of 5X (standard PI controller)

The adaptive Q-controller overcomes the error saturation problem. It automatically increases the effective Q-factor of the probe during scanning when the error between the oscillation amplitude A and the set amplitude A_{set} is close to the saturation limit (i.e. $A > A_{threshold}$). Augmenting the effective Q-factor of the probe increases its free-air oscillation amplitude and the magnitude of the error signal sent to the standard PI controller adjusting the Z-movements of the sample. As a result, the scanning system responds to the downward steps faster. This improves the overall quality of the profile and makes it possible to scan faster. Figure 6.6 shows the profile and the error signal of a single scan line for the scan speed of 5X when the adaptive Q-control is active. The undesired effects of the error saturation on the profile are significantly reduced with the adaptive Q-control. Note that, G_{set} in is set to zero so that Q_{set} is equal to the native Q-factor of the probe ($Q_{set} = Q_R$) and the Q-factor of the probe is only modified by the adaptive Q-controller when $A>A_{treshold}$.

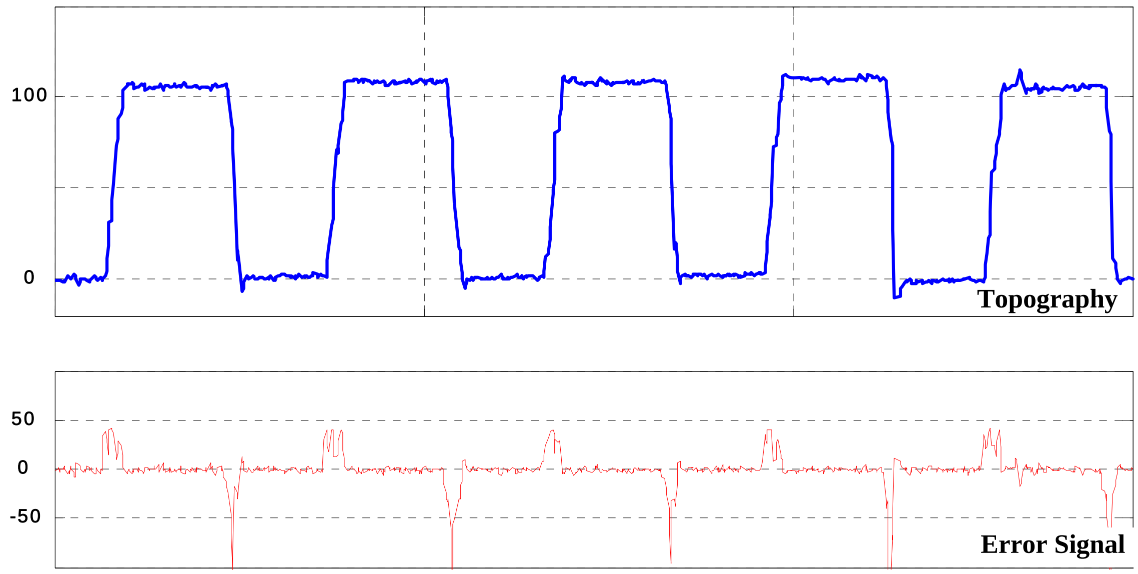

Figure 6.6: The scan profile and the error signal for the scan speed of 5X when adaptive Q-controller is active.

Figure 6.7 shows the effect of turning the adaptive Q-control on and off. The blue-colored line represents the RMS of the vibrometer output (in voltage) whereas red-colored line shows the value of the feedback gain G(t). Figure 6.7 (a) pinpoints the regions of error saturation where the error cannot exceed the maximum saturation amplitude (A_{set}-A_0). When the adaptive Q-controller is on, the G(t) is increased (and hence the Q-factor of the probe) automatically when the error saturation is detected. An increase in the Q-factor causes an increase in the vibration amplitude A (as well as the error signal A_{set}-A) and results in faster response of the controller as shown in figure 6.7 (b).

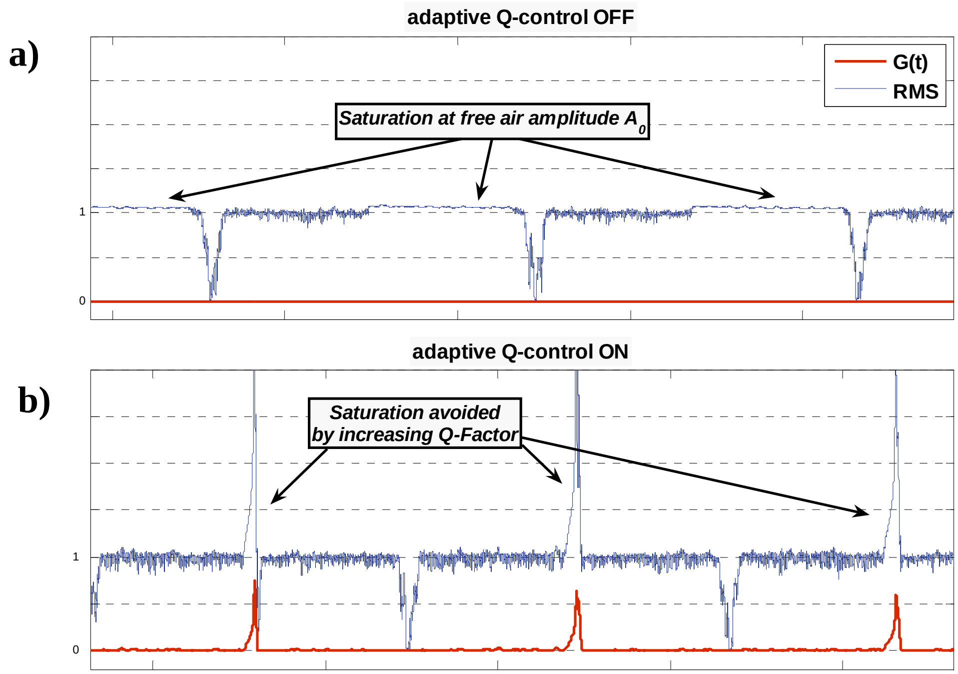

Figure 6.7: When the adaptive Q-controller is active, the feedback gain G(t) is increased automatically such that the error saturation is avoided.

In order to scan effectively at high speeds, the Q-factor of the probe can be reduced prior to scanning using the standard Q-control. Reducing the Q-factor of the probe amplifies the tapping forces applied by the probe tip to the sample. However, it is necessary to keep the tapping forces low when scanning soft samples in biological applications where high forces may easily damage the sample. In order to reduce the tapping forces, the ratio of A_{set}/A_0 can be increased, but this leads to the error saturation problem and detachment of the probe tip from the sample surface easily. In addition to increasing the scanning speed, adaptive Q-controller reduces the tapping forces by enabling higher set amplitudes (A_{set}) to be used for scanning. In Figure 6.8, the profiles scanned using the standard and the adaptive Q control is presented. In both (a) and (b), the Q-factor of the probe is reduced to the same low value of Q_{set} ($Q_{set} < Q_R$) to achieve higher scan speeds and the set amplitude (A_{set}) is set close to the free air amplitude A_0 to reduce the tapping forces. As shown in the Figure 6.8, the adaptive Q-control outperforms the standard Q-control.

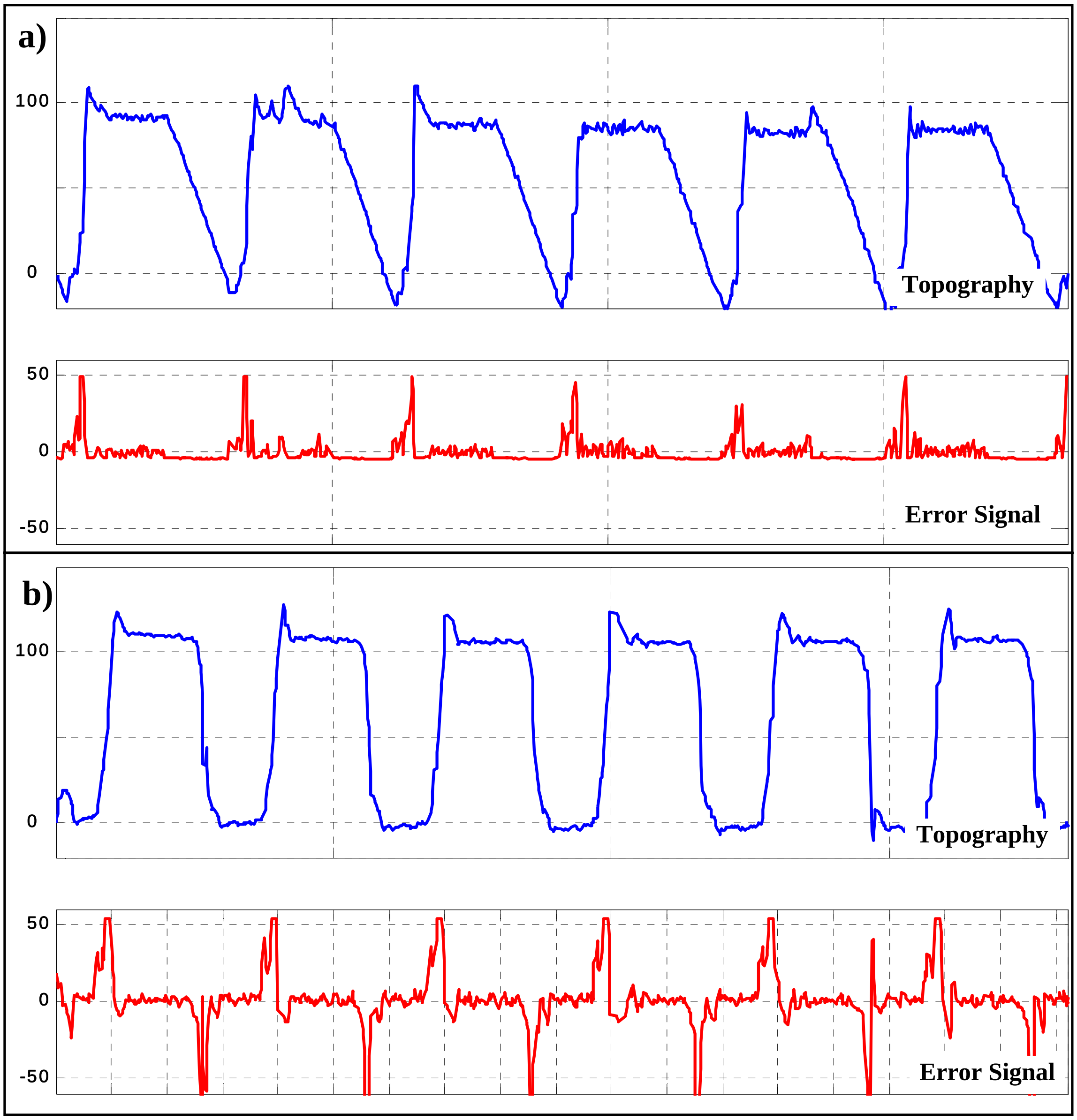

Figure 6.8: The scan profile and the error signal for the scan speed of 10X when the standard Q-controller (a) and the adaptive Q-controller (b) are employed. Note that Q_{set} is chosen lower than Q_R to increase the scan speed and A_{set} is set close to the free air amplitude A_0 to reduce the tapping forces.

Chapter 7

DISCUSSION and CONCLUSION

7.1 Discussion and Conclusion

In this work, the adaptive Q-control has been introduced and implemented. In order to test the performance of the proposed controller, an AFM set-up utilizing a LDV and a piezo-actuated bimorph probe has been constructed. Experiments with the AFM set-up show that adaptive Q-control increases the maximum achievable scan speed of the system while keeping the tapping forces low. Achieving these two benefits simultaneously using the standard Q-control is not possible due to the trade-off between the scanning bandwidth and the tapping forces. In order to scan a sample faster, the Q-factor of the probe must be decreased which increases the bandwidth of the probe. However, this may cause the probe to apply excessive tapping forces to the sample. In order to tap the sample lightly, either the Q-factor of the probe must be increased which increases the sensitivity of the probe but reduces the scan speed or the ratio of A_{set}/A_0 must be increased which causes error saturation. Such a scanning scenario is given in Chapter 6. The Q-factor of the probe is reduced and the ratio of A_{set}/A_0 is increased in the same scan to demonstrate the effectiveness of the adaptive Q-control over the standard Q-control. When the set amplitude A_{set} is close to the free air amplitude A_0, the error signal is weak and the response of the scan controller (i.e. PI controller) is slow. Moreover, the sensitivity of the probe is decreased and it cannot easily respond to the changes when the probe encounters a downward step. The resulting scan is highly unsatisfactory even when the standard Q-control is active (Figure 6.8a). However, the results obtained using the adaptive Q-control is better as shown in Figure 6.8b.

The technologies that enable us to modify the quality factor of the probe in real-time are the piezo layer on the cantilever and the analog signal processing circuit designed for modifying the Q-factor of the probe in real-time. The piezo actuation layer of the bimorph probe used in our system is much smaller in size and mass than a piezo stack typically used in standard AFM systems for vibrating the probe, therefore its response time is order of magnitude faster [46]. The wide bandwidth of the piezo actuation layer on the probe enables us to rapidly modify the effective Q-factor of the probe during the scanning when necessary. The new signal processing circuit adjusts the variable gain G(t) which is automatically controlled by an xPC Target for achieving real-time performance. In comparison, the gain in standard Q-controllers is fixed and set by the user prior to scanning and does not change throughout the scanning process. In adaptive Q-control, this gain is adjusted by the controller on the fly depending on the error in amplitude signal. If there is a tendency towards saturation in error, the controller increases the Q-factor of the probe rapidly to avoid the problem. Moreover, the LDV in our set-up is equipped with a velocity decoder and hence enables us to feed back the “true” vibration velocity of the probe to actuation signal in order to modify the effective damping of the probe. On the other hand, in typical AFM system utilizing photo sensors for measuring probe deflections, the measured displacement signal is first phase-shifted and then scaled to be used for velocity feedback when the standard Q-control is employed. Since the tip-sample interactions are nonlinear during tapping, the LDV equipped with a velocity decoder can provide more realistic velocity feedback than the conventional phase-shifting approach.

BIBLIOGRAPHY

[1] G. Binnig, C.F. Quate, C. Gerber, Atomic Force Microscope Physical Review Letters, 56, (1986), 930-933.

[2] Martin Y., Williams C.C., Wickramasinghe H.K., Atomic force microscope–force mapping and profiling on a sub 100-Å scale, Journal of Applied Physics, 61, (1987), 4723-4729.

[3] Albrecht T.R., Grütter P., Horne D., Rugar D., Frequency modulation detection using high-Q cantilevers for enhanced force microscope sensitivity, Journal of Applied Physics, 69, (1990), 668-673.

[4] Zhong Q., Imniss D., Kjoller K., Elings V.B., Fractured polymer/silica fiber surface studied by tapping-mode atomic force microscopy, Surface Science, 290, (1993), 688-692.

[5] Garcia R., Pérez R., Dynamic Atomic Force Microscopy Methods, Surface Science Reports, 47, (2002), 197-301.

[6] Rodriguez T.R., Garcia R., Theory of Q control in atomic force microscopy, Applied Physics Letters, (2003).

[7] San Paulo A., Garcia R., Biophysics Journal, 66, (2000), 1599.

[8] Anczykowski B., Cleveland J.P., Krüger D., Elings V., Fuchs H., Analysis of the interaction mechanisms in dynamic mode SFM by means of experimental data and computer simulation, Applied Physics A: Materials Science Processing, 66, (1998), 885.

[9] Sulchek T., Hsieh R., Adams J.D., Yaralioglu G.G., Minne S.C., Quate C.F., Cleveland J.P., Atalar A., Adderton D.M., High-speed tapping mode imaging with active Q-control for atomic force microscopy, Applied Physics Letters, 76, (2000), 1473.

[10] Hölscher H., Ebeling D., Schwarz U.D., Theory of Q-controlled dynamic force microscopy in air, Journal of Applied Physics, 99, (2006).

[11] Kokavecz J., Horvath Z.L., Mechler A., Dynamical properties of the Q-controlled atomic force microscope, Applied Physics Letters, 15, (2004), 3232.

[12] Tamayo J., Lechuga M., Decrease of the resonance bandwidth of micromechanical oscillators by phase control of the driving force, Applied Physics Letters, 82, (2003), 2919.

[13] Kokavecz J., Marti O., Heszler P., Mechler A., Imaging bandwidth of the tapping mode atomic force microscope probe, Physical Review B, 73, (2006).

[14] Sulchek, T., Yaralioglu, G. G., Quate, C. F., Minne, S. C. , Characterization and optimization of scan speed for tapping-mode atomic force microscopy, Review of Scientific Instruments, 73 (8), (2002), 2928-2936.

[15] Ebeling D., Hölscher H., Fuchs H., Anczykowski B., Schwarz U.D., Imaging of biomaterials in liquids: a comparison between conventional and Q-controlled amplitude modulation (‘tapping mode’) atomic force microscopy, Nanotechnology, 17, (2006), S221.

[16] Schaffer T.E., Cleveland J.P., Ohnesorge F., Walters D.A., Hansma P.K., Studies of vibrating atomic force microscope cantilevers in liquids, Journal of Applied Physics, 80, (1996), 3622.

[17] Anczykowski B., Krüger D., Fuchs H., Cantilever dynamics in quasinoncontact force microscopy: Spectroscopic aspects, Physical Review B, 53, (1996), 15485.

[18] Stark R.W., Schitter G., Stark M., Guckenberger R., Stemmer A., State-space model of freely vibrating and surface-coupled cantilever dynamics in AFM, Physical Review B, 69, (2004).

[19] Lobontiu N., Garcia E., Two microcantilever designs: lumped-parameter mode for static and modal analysis, Journal of Microelectromechanical Systems, 13, (2004), 41.

[20] Wang L., Analytical descriptions of the tapping-mode atomic force microscopy response, Applied Physics Letters, 73, (1998), 3781.

[21] Wang L., The role of damping in phase imaging in tapping mode atomic force microscopy, Surface Science, 429, (1999), 178.

[22] San Paulo A., Garcia R., Unifying theory of tapping-mode atomic force microscopy, Physical Review B, (2002).

[23] Spalka M.V., Chen D.J., Cleveland J.P., Linearity of amplitude and phase in tapping-mode atomic force microscopy, Physical Review B, 61, (2000), 1106.

[24] Cleveland J.P., Anczykowski B., Schmid A.E., Elings V.B., Energy dissipation in tapping-mode atomic force microscopy, Applied Physics Letters, 72, (1998), 2613.

[25] Ashhab M., Salapaka M.V., Dahleh M., Mezic I., Dynamical analysis and control of microcantilevers, Automatica, 35, (1999), 1663.

[26] Garcia R., San Paulo A., Dynamics of vibrating tip near or in intermittent contact with a surface, Physical Review B, 61, (2000), R13381.

[27] De Pablo P. J., Colchero J., Gomez-Herrero J., Baro A. M., Schaefer D. M., Howell S., Walsh B., Reifenberger R., Adhesion maps using scanning force microscopy techniques, The Journal of adhesion, 71, (1999), 339-356.

[28] M. Sitti and H. Hashimoto, Teleoperated touch feedback from the surfaces at the nanoscale: modeling and experiments, Mechatronics, IEEE/ASME Transactions on, 8, (2003), 287-298.

[29] Johnson K.L., Contact Mechanics, Cambridge University Press, (1985).

[30] Muller V.M., Yushchenko V.S., Derjagurin B.V., On the influence of molecular forces on the deformation of an elastic sphere and its sticking to a rigid plane, Journal of Colloid and Interface Science, 77, (1980), 91.

[31] Derjagurin B.V., Muller V.M., Toporov Y.P., Effects of contact deformations on the adhesion of particles, Journal of Colloid Science, 53, (1975), 314.

[32] Burnham N.A., Behrend O.P., Oulevey F., Gremaud G., Gallo P.J., Gourdon D., Dupas E., Kulik A.J., Pollock H.M., Briggs G.A.D., How does it tap?, Nanotechnology, (1997).

[33] Johnson K.L., Kendall K., Roberts A.D., Surface energy and contact of elastic solids, Proceedings of the Royal Society of London: Series A, 324, (1971), 301.

[34] Sperling G., Eine Theorie der Haftung von Feststoffteilchen an festern Köpern, Ph.D. Thesis, T H Karlsruhe, (1964).

[35] Maugis D., Adhesion of spheres: The JKR-DMT transition using a Dugdale Model, Journal of Colloid and Interface Science, 150, (1992), 243.

[36] Maugis D., Gauthier-Manuel B., Journal of Adhesion Science and Technology, 8, (1994), 1311.

[37] Dugdale D.S., Yielding of steel sheets containing slits, Journal of Mechanics and Physics of Solids, 8, (1960), 100.

[38] Morrow C., Lovell M., Ning X., A JKR-DMT transition solution for adhesive rough surface contact, Journal of Physics D: Applied Physics, 36, (2003), 534.

[39] Shull K.R., Contact mechanics and the adhesion of soft solids, Materials Science and Engineering, 36, (2002), 1.

[40] Tamayo J., Humphris A.D.L., Miles M., Piconewton regime dynamic force microscopy in liquid, Applied Physics Letters, 77, (2000), 582.

[41] Tamayo J., Humpris A.D.L., Owen R.J., Miles M.J., High-Q dynamic force microscopy in liquid and its application to living cells, Biophysical Journal, 81, (2001), 526.

[42] Veeco Instruments. Probes Catalog, (2006).

[43] Kodera N., Sakashita M., Ando T., Dynamic proportional-integral-differential controller for high-speed atomic force microscopy, Review of Scientific Instruments, 77, (2006)

[44] Burnham N. A., Chen X.,Hodges C. S., Matei G. A., Thoreson E. J., Roberts C. J., Davies M. C. and Tendler S. J. B., Comparison of calibration methods for atomic-force microscopy cantilevers, 14, (2003), 1-6,.

[45] Cleveland, J.P., S. Manne, D. Bocek and P.K. Hansma., A Nondestructive Method for Determining the Spring Constant of Cantilevers for Scanning Force Microscopy, Review of Scientific Instruments, 64, (1993), 403-405.

[46] Manalis S. R., Minne S. C., Atalar A., and Quate C. F., Contact imaging in the atomic force microscope using higher order flexural mode combined with a new sensor, Review of Scientific Instruments, 67, (1996), 3294.